

Full-lifetime simulations of multiple unequal-mass planets across all phases of stellar evolution

Dimitri Veras^{1*}, Alexander J. Mustill², Boris T. Gänsicke¹, Seth Redfield³, Nikolaos Georgakarakos⁴, Alex B. Bowler¹, Maximillian J.S. Lloyd¹

¹*Department of Physics, University of Warwick, Coventry CV4 7AL, UK*

²*Lund Observatory, Department of Astronomy and Theoretical Physics, Lund University, Box 43, SE-221 00 Lund, Sweden*

³*Astronomy Department and Van Vleck Observatory, Wesleyan University, Middletown, CT 06459-0123, USA*

⁴*New York University Abu Dhabi, Saadiyat Island, P.O. Box 129188, Abu Dhabi, UAE*

Accepted 2016 February 25. Received 2016 February 25; in original form 2016 January 27

ABSTRACT

We know that planetary systems are just as common around white dwarfs as around main sequence stars. However, self-consistently linking a planetary system across these two phases of stellar evolution through the violent giant branch poses computational challenges, and previous studies restricted architectures to equal-mass planets. Here, we remove this constraint and perform over 450 numerical integrations over a Hubble time (14 Gyr) of packed planetary systems with unequal-mass planets. We characterize the resulting trends as a function of planet order and mass. We find that intrusive radial incursions in the vicinity of the white dwarf become less likely as the dispersion amongst planet masses increases. The orbital meandering which may sustain a sufficiently dynamic environment around a white dwarf to explain observations is more dependent on the presence of terrestrial-mass planets than any variation in planetary mass. Triggering unpacking or instability during the white dwarf phase is comparably easy for systems of unequal-mass planets and systems of equal-mass planets; instabilities during the giant branch phase remain rare and require fine-tuning of initial conditions. We list the key dynamical features of each simulation individually as a potential guide for upcoming discoveries.

Key words: minor planets, asteroids: general – stars: white dwarfs – methods: numerical – celestial mechanics – planet and satellites: dynamical evolution and stability – protoplanetary discs

1 INTRODUCTION

Nearly 100 planets are known to orbit giant stars¹, and signatures of planetary systems have been detected at over 1000 white dwarfs. This latter number is obtained through observed planetary debris in white dwarf atmospheres (Zuckerman et al. 2003; Dufour et al. 2007; Zuckerman et al. 2010; Kleinman et al. 2013; Koester et al. 2014; Gentile Fusillo et al. 2015; Kepler et al. 2015, 2016). About 40 of these white dwarfs contain compact ($\approx 0.6 - 1.2R_{\odot}$) planetary debris discs (see Farihi 2016 for a review), and one hosts at least six transiting planetesimals (WD 1145+017: Vanderburg et al. 2015; Croll et al. 2016; Gänsicke et al. 2016; Rappaport et al. 2016; Xu et al. 2016). Also, planets around two other white dwarfs have been observed (WD 0806-661 b: Luhman et al. 2011, and PSR

B1620-26AB b: Sigurdsson et al. 2003). Although the architectures of most white dwarf planetary systems remain unknown, these statistics demonstrate that the study of post-main-sequence planetary systems has entered a new era, one where we can begin to investigate population-wide trends as well as key individual systems. N -body simulations of multi-planet systems represent a vital probe into their history and future, revealing insights about their formation and fate.

However, accurately performing multi-body simulations across different phases of stellar evolution remains challenging. For bodies much smaller than planets, including gravity alone is likely to be insufficient (see Fig. 2 of Veras 2016). Asteroids within about 7 au of a main sequence star could be spun up to fission during the giant branch phase of stellar evolution (Veras et al. 2014a) due to intense radiation. Asteroids further away could have their orbits changed due to another radiation-based effect: the Yarkovsky drift (Veras et al. 2015a). Further, the stellar wind could induce drag on asteroids and pebbles

* E-mail: d.veras@warwick.ac.uk

¹ www.lsw.uni-heidelberg.de/users/sreffert/giantplanets.html

(Dong et al. 2010; Veras et al. 2015a), and sublimation of volatile substances on these objects could change their orbits (Veras et al. 2015b) and/or launch ejecta, as speculated in WD 1145+017 (Vanderburg et al. 2015; Croll et al. 2016; Gänsicke et al. 2016; Rappaport et al. 2016; Xu et al. 2016).

Even restricting simulations to planets presents challenges: (i) Tidal effects between planets and their parent stars can destroy or alter the planets, but just how remains an open question (see Sec. 5 of Veras 2016 for a review). Giant branch (GB) stars harbour radii that extend to several au, and planets too close to their parent stars may hence be engulfed on both the red giant branch (RGB) phase (e.g. Villaver et al. 2014) and the asymptotic giant branch (AGB) phase (Mustill & Villaver 2012). Nevertheless, only about half of the currently known exoplanets will likely be engulfed (Nordhaus & Spiegel 2013), and observational biases against finding planets at large separations imply that the actual fraction is much less. (ii) Computational limitations hinder explorations with long main-sequence lifetimes or planets on close-in orbits. Only recently (Veras & Gänsicke 2015) have 14 Gyr (the current age of the Universe) simulations with main sequence progenitor masses under $3M_{\odot}$ (most white dwarf progenitors had masses between about $1.5M_{\odot}$ and $2.5M_{\odot}$; Koester et al. 2014) been carried out for ensembles of multi-planet systems², as previous attempts (Duncan & Lissauer 1998; Debes & Sigurdsson 2002; Veras et al. 2013a; Mustill et al. 2014) did not achieve this coverage.

Nevertheless, up until now full-lifetime simulations of multi-planet systems have been restricted to equal-mass planets. Although this assumption significantly helps constrain the available parameter space to explore, real systems exhibit a variance of planetary masses of a few percent to many orders of magnitude. Further, previous studies have predominately modelled Jupiter-mass planets, which are rarer than terrestrial planets (Cassan et al. 2012; Winn & Fabrycky 2015). Further, no published study has simulated multiple planets with test particles.

Here, we break these barriers, and perform a suite of 14 Gyr simulations of unequal-mass planets, occasionally including test particles, in order to explore the consequences and resulting trends. In Section 2, we describe our setup. Section 3 details the classification scheme for our results, and the results themselves. We discuss the implications in Section 4, and conclude in Section 5.

Appendix A is our simulation database. Each row of each table corresponds to one simulation, and within each row we present the salient dynamical features.

2 SIMULATION SETUP

Simulations of planetary systems through multiple stages of stellar evolution require both the star and planets to be treated self-consistently as a function of time.

² A few individual planetary systems, or putative planetary systems, have been modelled with simulations spanning multiple phases of evolution: HU Aqr (Portegies Zwart 2013) and NN Ser (Mustill et al. 2013).

2.1 Numerical codes

Here we have used an updated version of the code from Veras et al. (2013a), Mustill et al. (2014), Veras et al. (2014b) and Veras & Gänsicke (2015), which combines planetary and stellar evolution. The stellar evolution is computed from SSE (Hurley et al. 2000), which is more than sufficiently accurate for our purposes. If we instead desired to trace more detailed characteristics of a particular star, like its chemical profile, then perhaps a code like the increasingly utilized MESA (Paxton et al. 2011, 2015) would be more suitable. However, here we need only the mass and radius evolution of the star, and did not model any particular known system; we ignored radiative effects, which are negligible for the types of planets we simulated.

The output from SSE was ported directly into a heavily modified version of the MERCURY planetary evolution code, originally from Chambers (1999). Our version of MERCURY used the Bulirsch-Stoer integrator throughout the simulation, ensuring accurate treatment of potential close encounters. We adopted a tolerance value of 10^{-13} . Stellar mass and radius changes were interpolated within each Bulirsch-Stoer timestep, helping to ensure accuracy. Stars which engulfed planets throughout the course of the simulations had masses which were increased accordingly. Our output frequency was 1 Myr; a shorter frequency would have prohibitively slowed down our simulations. As is the MERCURY default, any collisions between planets were treated as purely inelastic. Further, our modified code allowed for the tracking of the minimum orbital pericentre of all surviving planets, and adopted a standard Hill ellipsoid for the solar neighbourhood (Veras & Evans 2013; Veras et al. 2014c) to accurately track ejections.

2.2 Stellar properties

The enormous parameter space of our computationally-demanding simulations forced us to adopt a single type of star for our simulations. Our star contained a physically-motivated stellar mass of $2.0M_{\odot}$ on the main sequence. The present-day population of white dwarfs, with average masses ranging from about $0.60M_{\odot}$ to $0.65M_{\odot}$ (Liebert et al. 2005; Falcon et al. 2010; Tremblay et al. 2013) corresponds to main sequence A- and F-star progenitors (see Fig. 3 of Veras 2016), from which $2.0M_{\odot}$ is an appropriate value from the initial-to-final mass relation (Catalán et al. 2008; Kalirai et al. 2008; Casewell et al. 2009; Koester et al. 2014). This value coincidentally also marks (i) the point beyond which the planet occurrence rate falls off (Reffert et al. 2015) and (ii) a transition in evolutionary sequence due to stellar mass; below $2.0M_{\odot}$ a star would continue ascending the RGB until it undergoes a core helium flash, which changes the amount of mass lost and radius along the RGB. Lower-mass stars have larger radii and greater mass loss. Regardless, the greatest mass loss (by several orders of magnitude) and radius changes occur along the AGB even for values within a few $0.1M_{\odot}$ of $2.0M_{\odot}$.

The evolution of the star is illustrated in Fig. 1, characterized in Table 1 and described in this paragraph. Our $2.0M_{\odot}$ star was assumed to have Solar metallicity, and remained on the main sequence for 1.1735 Gyr. Along

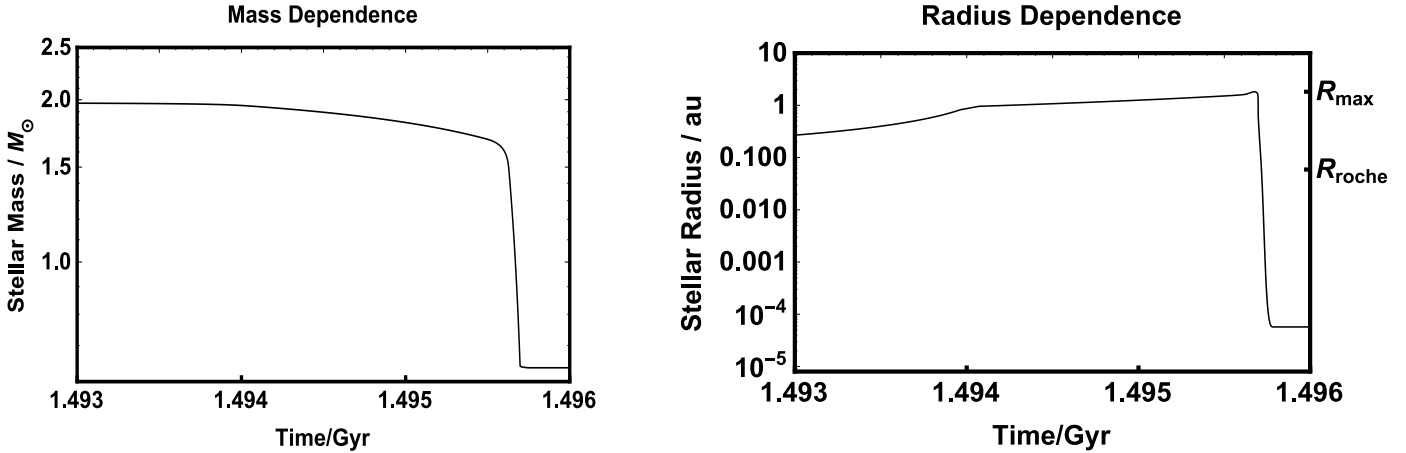


Figure 1. The mass (*left panel*) and radius (*right panel*) evolution of the star used in this study, during the tip of the AGB phase and when the white dwarf is born (at the start of the EWD= “early white dwarf” phase). Marked on the right panel is the maximum AGB radius (R_{\max}) and the white dwarf Roche radius (distance) adopted in this study (R_{roche}).

Table 1. Time at the beginning of each phase (MS = main sequence, GB = giant branch, EWD = early white dwarf, LWD = late white dwarf) and the total mass lost during those phases. The LWD phase lasts until the end of the simulations (14 Gyr).

	MS	GB	EWD	LWD
Start Time (Gyr)	0.0	1.1735	1.4958	1.5958
Mass Lost (M_{\odot})	0.0	1.363	0.0	0.0

the RGB, the star lost mass according to the traditional³ Reimers mass loss prescription, with a numerical coefficient of 0.5. The star stayed on the RGB for 23 Myr and lost $0.002M_{\odot}$ during that time, while expanding its radius out to 0.13 au. Afterwards, the star contracted to a radius of 0.04 au. The AGB phase began at 1.4894 Gyr, and lasted for only 6.4 Myr. However, during this time, the star lost $1.338M_{\odot}$ and expanded its radius out to 1.82 au; see Fig. 1. Finally, the star ended its evolution as a white dwarf formed with a mass of $0.6365M_{\odot}$ and a radius of 5×10^{-5} au.

Varying the stellar mass within the code is nearly equivalent to assuming that the star loses mass isotropically. This assumption is excellent for orbiting bodies within a few hundred au (Veras et al. 2013b). Because the planets are assumed to be point masses, they do not accrete any of the stellar mass and the isotropic assumption is maintained; see Sec. 4 of Veras (2016) for more details. This type of stellar mass decrease, however, does not consider the lag time between the ejecta passing beyond two different orbits. However, this effect should be negligible; see section 2 of Payne et al. (2016) for quantification.

A planet that ventures into the vicinity of the white dwarf might be disrupted or destroyed. This “vicinity” may extend to a few hundred times the white dwarf radius. The critical radius at which disruption occurs (known as the Roche radius), however, is dependent on the planet’s shape,

³ Schröder & Cuntz (2005) provided an improved, physically-motivated version of this prescription, but one that requires knowledge of further details (surface gravity, temperature) about the star.

composition, spin state, orbital state, and whether one considers disruption to mean cracking, deforming or dissociating. This ambiguity is compounded by the fact that no study has yet modelled the disruption of a planet around a white dwarf⁴. Although the disruption of rubble pile asteroids around white dwarfs has been numerically modelled (Debes et al. 2012; Veras et al. 2014d), the situation with planets is fundamentally different. These uncertainties prompted us to rescale the white dwarf radius within the simulations to a value corresponding to its fiducial Roche, or disruption, radius: $1.27R_{\odot} \approx 0.0059$ au, where R_{\odot} is the Sun’s radius. This value roughly represents the outer extent of the compact debris discs which surround white dwarfs (see Farihi 2016 for a review). These discs are assumed to be composed of disrupted fragments and particles.

2.3 Planet properties

Our goal is to simulate planetary systems that become unstable. Instability in planetary systems is likely to be common, as demonstrated by the Grand Tack model (Pierens & Raymond 2011; Walsh et al. 2011; O’Brien et al. 2014; Izidoro et al. 2015) and the Nice model (Gomes et al. 2005; Morbidelli et al. 2005; Tsiganis et al. 2005; Levison et al. 2011) for our solar system, and by the potential future instability of packed exoplanetary systems, which are prevalent (recent examples include Barclay et al. 2015 and Campante et al. 2015; see also Pu & Wu 2015)⁵. Further, metal-polluted white dwarfs, which comprise between one-quarter and one-half of all Milky Way white dwarfs (Zuckerman et al. 2003, 2010; Koester et al. 2014),

⁴ Main-sequence disruption investigations (Guillochon et al. 2011; Liu et al. 2013) suggest that the assumed structure of the planet plays a vital role, as well as how much mass is sheared off during each close passage to the star.

⁵ Rarely has the future non-secular evolution of planetary systems throughout the entire main sequence been achieved with N -body numerical integrations. Consequently, the prospects for future instability of the currently-observed exoplanetary systems is generally unknown.

Table 2. Mass ratios of different planets (J = Jupiter, S = Saturn, N = Neptune, U = Uranus). These ratios are equivalent to those of the planets which are scaled-down in mass (\bar{J} , \bar{S} , \bar{N} , \bar{U}).

	J	S	N	U
J	1	0.30	0.054	0.046
S	3.34	1	0.18	0.15
N	18.53	5.55	1	0.85
U	21.87	6.55	1.18	1

are thought to arise from planetary system instability after the star has become a white dwarf.

We consider simulation suites of primarily 4-planet systems in order to facilitate comparison with the equal-mass cases of Veras & Gänsicke (2015), although we also ran smaller samples of six- and eight-planet systems. We also adopted simulations that each contained four planets and 12 test particles. Each test particle represents a planet or asteroid which is both (i) small enough relative to the nonzero-mass planets to not affect them, and (ii) large enough to not be affected by radiation, which is not modelled. One example is four giant planets with test particles represented by Earths. Large asteroids with radii above about 100 km may also be represented as test particles, because the effect of radiation for objects of these sizes may be negligible (see eqs. 108 and 110 of Veras et al. 2015a and eq. 1 of Veras et al. 2014a).

For our nonzero-mass substellar bodies, we adopted eight types of planets: Jupiter, Saturn, Uranus, Neptune (which we refer to as “giant planets”), and all of their analogues scaled down in mass by a ratio of $M_{\text{Jupiter}}/M_{\oplus} \approx 317.8$ (which we refer to as “terrestrial planets”). The mass scaling effectively transforms Jupiter into Earth, and the other giant planets into three sub-Earth mass companions. The scaled-down planets allow us to provide direct dynamical comparisons while keeping the mass ratios amongst the planets the same. These terrestrial planets also arguably yielded the most interesting results. We adopted giant planet densities which reflect those of Jupiter, Saturn, Uranus and Neptune. The density of all the scaled-down planets was set to the density of the Earth.

We henceforth denote the giant planets as J, S, U, N, and the terrestrial planets as \bar{J} , \bar{S} , \bar{U} , and \bar{N} . All of the planetary system combinations that we adopted per simulation are presented in the Appendix. For perspective on the relative mass values, see Table 2. Test particles are by definition massless, and can reasonably represent objects (whether they be planets, asteroids or pebbles) which are at least two or three orders of magnitude less massive than the non-zero mass bodies in the simulation. Also, $M_{\text{Jupiter}}/M_{\odot} = 9.54 \times 10^{-4}$ and $M_{\oplus}/M_{\odot} = 3.00 \times 10^{-6}$.

Our choices for initial orbital eccentricities, inclinations, orbital angles, and innermost semimajor axis follow those of previous studies (Mustill et al. 2014; Veras & Gänsicke 2015) and their justifications are only briefly repeated here. All planets are assumed to be on initially circular orbits and have small inclinations randomly selected from a uniform distribution from -1° to 1° . Adopting strictly non-coplanar planets prevent an unnaturally high rate of planet-planet collisions, which occurred in Veras et al. (2013a). Imposing non-zero initial eccentricities would change (speed up) instability timescales; we did not do so in order to facilitate

comparisons with previous studies. The innermost planet semimajor axis was always set at 5 au to prevent AGB star-planet tides from playing a role in the evolution (see Fig. 7 of Mustill & Villaver 2012) before any potential instability occurs. Further, 5 au is a particularly appropriate value considering that Jupiter lies at 5.2 au from the Sun and is the closest of the four giant planets in our Solar system.

The much trickier initial parameter to determine was the initial spacing of the planets. For equal-mass planets, the link with initial spacing and instability timescales has a now-substantial history (see Davies et al. 2014 for a review), particularly with the application of the mutual Hill radius as the separation unit. However, no widely-used formalism exists with unequal-mass planets. Consequently, for lack of better proven alternatives, we applied the mutual Hill radius to our architectures here. Multiple definitions of this parameter exist: we adopted eq. (4) of Smith & Lissauer (2009) in order to maintain consistency and provide meaningful comparisons with Veras & Gänsicke (2015):

$$a_{i+1} = a_i \left[1 + \frac{\beta}{2} \left(\frac{m_i + m_{i+1}}{3(m_{\star} + \sum_{k=1}^{i-1} m_k)} \right)^{1/3} \right] \times \left[1 - \frac{\beta}{2} \left(\frac{m_i + m_{i+1}}{3(m_{\star} + \sum_{k=1}^{i-1} m_k)} \right)^{1/3} \right]^{-1}. \quad (1)$$

In this equation, a and m refer to mass and initial semimajor axis, and the subscripts ascend in order of increasing distance from the star. The important quantity β is the number of mutual Hill radii. In order to determine meaningful values of β for the different architectures we considered, we performed exploratory preliminary suites of simulations. We found that a wide range ($\beta = 6 - 14$) was necessary to implement depending on the architecture considered. The specific values used for each architecture are listed in Tables A1-A13.

Having established the planet locations, we then considered where potential test particles would reside. We distributed our 12 test particles uniformly in a ring at 2.5 au from the star. This choice is in the spirit, if not the details, of the asteroid belt. In our Solar system, the largest objects in this belt (with sizes greater than 100 km) are unlikely to be influenced by Solar giant branch radiation, and will neither be engulfed by the Solar giant. Recall that these particles could instead represent Mars, which also will survive the Sun’s post-main-sequence evolution, despite being located at about 1.5 au (Schröder & Connors 2008).

2.4 Additional physics

Besides radiation, other physics that could play a role in planetary system evolution include star-planet tides and general relativity. A planet which is perturbed on an orbit with a pericentre that lies just outside of the Roche radius may be tidally circularized. The particulars of this process are highly dependent on the composition of the approaching planet and the evolutionary stage of the star; all our bodies are point-masses with no assumed composition. The variation in tidal circularization behaviour and timescale due

to composition is so great (Henning & Hurford 2014) that any meaningful exploration would require a dedicated study, which we do not perform here. Our simulations here illustrate preconditions for this tidal interaction to occur.

General relativity changes the rate of the argument of periastron for close-in bodies, and hence can by itself trigger instability in multi-planet systems (e.g. Veras & Ford 2010). Consequently, we have included the effects of general relativity in our simulations through our updated code.

2.5 Running time

We attempted to run all our simulations for 14 Gyr, which represents a Hubble time and is the current age of the Universe. We succeeded in over 90% of cases, the exceptions (which are all noted in the Appendix tables) being systems where a planet or test particle was perturbed close enough to the star to sufficiently slow down the simulations. We only report simulations which ran for at least 1.9 Gyr (recall that our star becomes a white dwarf after about 1.5 Gyr), in order to give a flavour of what the evolution is like on all of the main sequence, giant branch, and early white dwarf phases.

3 RESULTS

We present results for over 450 simulations, and have visually inspected the output and evolution of each one. They are partitioned into groups of up to four simulations such that each group member has the same (i) initial ordering and type of masses (such as $\bar{N}\bar{U}\bar{J}\bar{S}$ in order of increasing distance from the star), and (ii) value of β . Within these groups the initial orbital angles and inclinations are different.

We report the results of every simulation in Tables A1-A13, one per row, with particular attention to the stellar phases at which various events occurred rather than the specific times. This format allows one to determine qualitative trends easily amongst the many-dimensional parameter space, and acts as a handy reference for setting up future simulations if one has a desired outcome or set of initial conditions (perhaps based on a known exosystem) in mind.

In this section, we describe the data which is presented in the tables (Subsection 3.1), illustrate some representative and interesting examples (Subsection 3.2), list various system outcomes and behaviours which our simulations show to be possible (Subsection 3.3), and analyze the general trends from the tables (Subsection 3.4).

3.1 Description of table columns

In all tables, the first column (“Sim #”) provides a designation for each simulation for easy reference. The second column (“Setup”) provides the initial order and type of planets in each simulation. We reiterate that J, S, U, N, \bar{J} , \bar{S} , \bar{U} , and \bar{N} , respectively refer to planets which have the same masses of Jupiter, Saturn, Uranus, Neptune, and versions of those planets with masses scaled down by a factor of about 318 (thereby transforming Jupiter into Earth). All simulations in Tables A1-A11 contain four planets each. The last two tables (A12-A13) contain systems with four, six and eight

planets. The third column (“ β ”) refers to the number of mutual Hill radii between the planets, as defined from eq. (4) of Smith & Lissauer (2009).

Starting from the fourth column (“Unpack”) we characterize the timing of events in the evolution of the planetary system. We adopt designations for different phases of stellar evolution: MS (main sequence), GB (giant branch), EWD (“early white dwarf” that corresponds to stars that have become white dwarfs within the last 100 Myr), and LWD (“late white dwarf” stars which became white dwarfs over 100 Myr ago). We split up the white dwarf phase because the intense mass loss at the tip of the AGB phase often triggers slightly-delayed instability, which commonly manifests itself in white dwarfs whose cooling age (the time since becoming a white dwarf) is less than about 100 Myr. In effect, such systems are dynamically resetting themselves and hence feature instability at “early” times, just as we would expect from a planetary system recently born out of a Solar nebula. Precisely then, the MS phase corresponds to times between 0 and 1173.576 Myr, while the GB phase corresponds to times between 1173.576 Myr and 1495.783 Myr. At 1495.783 Myr, the EWD phase begins and lasts until 1595.783 Myr. The star then spends the remainder of its life on the LWD phase.

The fourth column itself (“Unpack”) displays the phase during which the system became unpacked. If the system never became unpacked, then the space is left blank. We define “unpacked” as the moment that either (i) two non-zero mass planets cross orbits, or (ii) an instability occurs. We define instability as an occurrence when two bodies collide with one another, or one body escapes the system. The collision could come in the form of a star-planet collision (when the planet is said to be engulfed in the star) or a planet-planet collision. Note also that the moment of escape may occur several Myr after the actual interaction which triggered the movement, because the Hill ellipsoid of the system typically lies at about 10^5 au from the star.

The fifth column (“# Surv”) indicates the number of non-zero mass planets which remained in the system by the end of the simulation. Those planets which do not survive are characterized in the next three columns (“Engulf”, “Eject” and “Collision”), which indicate respectively when a planet intersects with the stellar radius, is ejected from the system, or hits another planet. Recall that the white dwarf stellar radius is enhanced from its true value. The columns all indicate the phase in which an instability occurred, along with the planet(s) involved in the instability in the subscripts. The subscript numbers correspond to the planet order from the “Setup” column. Each instability is indicated by a single listed entry. The subscripts in each “Collision” entry indicate the two planets involved in the collision.

The column (“ $< R_{\max}$ ”) lists any non-zero mass planet that survived for the entire simulation and was perturbed into an orbit along the EWD or LWD phase whose pericentre was within the star’s maximum AGB radius (1.82 au). The subscript indicates the smallest planet-white dwarf distance achieved.

The column, labelled “TPs Eng”, does not exist in the final two tables (A12-A13). The column indicates when test particles were included in the simulations (a blank space means no test particles), and provides some information about them. The first and second numbers given are the

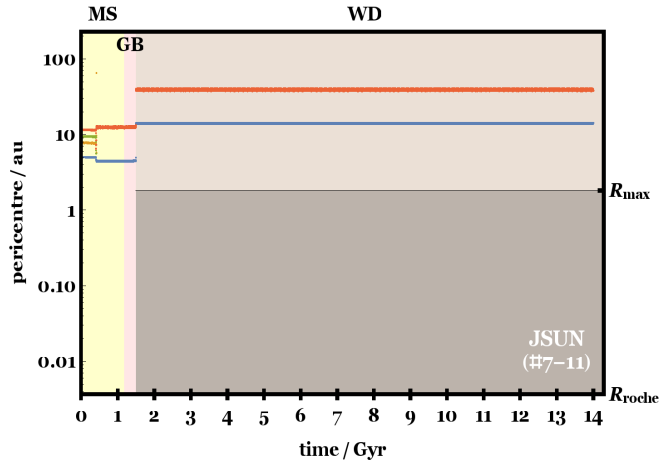


Figure 2. A characteristic outcome for the full-lifetime evolution of four giant planets: unpacking and instability on the main sequence, followed by stability. Note that the surviving two planets expand their orbits due to giant branch mass loss at 1.49 Gyr. The values of R_{\max} and R_{Roche} on the right axis indicate the maximum stellar AGB radius (1.82 au) and an approximate value of the disruption radius of white dwarf (0.0059 au). Shown is JUUU simulation #1-19 (Table A1).

amounts of test particles (out of 12) that were engulfed by the star during the EWD and LWD phases, respectively.

The final column lists relevant notes which are in the table captions.

3.2 Specific cases

Now we present some specific examples of evolutionary sequences.

3.2.1 Standard giant planet evolution

Consider first simulation #1-19 (in Table A1), whose evolution is shown in Fig. 2. The system initially consists of an inner Jupiter-mass planet (blue, at 5 au) followed by three Uranus-mass planets (JUUU), separated by $\beta = 8$. The system unpacks on the main sequence, and both the second and third planets (Uranuses) are ejected sometime during this phase. The two remaining planets have their orbits expanded due to mass loss at the end of the GB phase, remaining stable through this process and for the remainder of the simulation. Neither achieved an orbit that took it to within 1.82 au ($= R_{\max}$) of the white dwarf, and their pericentres remain nearly constant.

3.2.2 Squeezed solar system analogue – giant planets

Next consider a Solar system analogue architecture (JSUN and $\beta = 7$) from Table A7. Simulation #7-11, shown in Fig. 3, features Neptune and Uranus being ejected at 10.3 Myr and 18.5 Myr (effectively immediately), which is not discernable on the plot. The remaining Jupiter and Saturn mutually perturb each other so that their pericentres vary significantly (over 1 au in each case) throughout the main sequence.

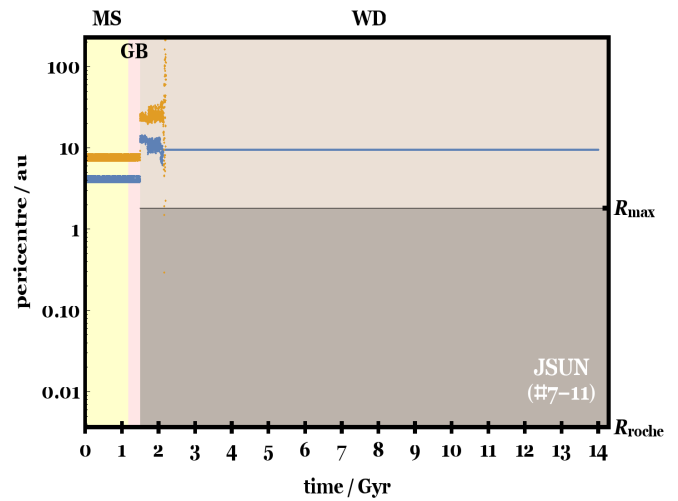


Figure 3. Evolution of a Solar-system analogue (JSUN) that immediately ejects Uranus and Neptune and keeps Saturn bound until the star is 2.2 Gyr old, which is 0.7 Gyr into the white dwarf phase. Only Jupiter survives for this particular evolution, which is simulation #7-11 (Table A7).

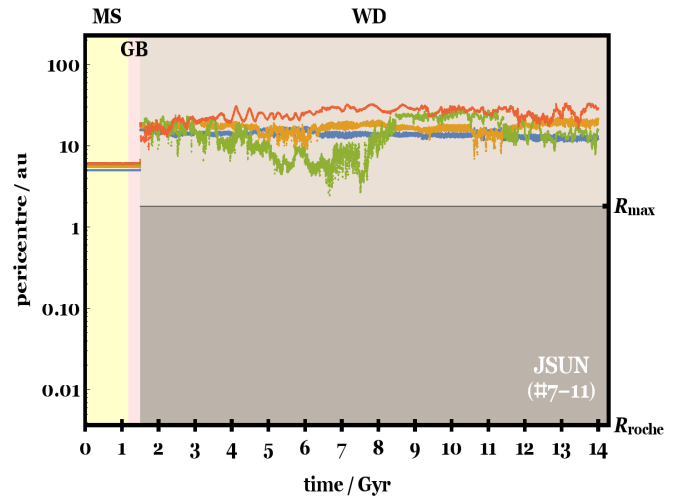


Figure 4. Unpacking of a set of terrestrial planets at the start of the white dwarf phase. The planets (JSUN) are scaled-down versions of Jupiter, Saturn, Uranus and Neptune, with the mass reduced by a factor of about 318, which transforms Jupiter into the Earth. All four planets remain stable, meander, and survive until the end of the simulation. Shown is simulation #7-40 (Table A7).

The orbital expansion causes the two-planet stability threshold (see Debes & Sigurdsson 2002, Veras et al. 2013a and Voyatzis et al. 2013) to be passed or at least skirted, leading to delayed instability on the white dwarf phase. The result is that at 2.2 Gyr, Saturn is ejected. Jupiter remains the lone survivor.

3.2.3 Solar system analogue – terrestrial planets

Alternatively, simulation #7-40 ($\beta = 11$, and Fig. 4) illustrates one evolutionary sequence for the scaled-down (by a mass factor of 318) versions of Jupiter, Saturn, Uranus and Neptune ($\bar{J}\bar{S}\bar{U}\bar{N}$) – effectively transforming them into terrestrial-mass planets. The system does not unpack until the EWD phase, but never becomes unstable. The resulting meandering causes the scaled-down Uranus (green) to achieve an orbital pericentre of just 2.47 au (less than half of any planet’s initial pericentre) at 6.67 Gyr.

3.2.4 Terrestrial planet pericentre repacking

Another example of a long-term stable terrestrial system, but one that becomes unpacked immediately, is from simulation #9-39 ($\bar{U}\bar{N}\bar{J}\bar{S}$ – blue, orange, green, red – from Table A9 and left panel of Fig. 5). This simulation contains two notable features: (i) the inward radial incursion of \bar{U} to a few au at around 8 Gyr (the first such radial incursion during the entire evolution), and (ii) the “re-packing” of the orbital pericentres beyond 8 Gyr. At this time, the system becomes orderly (but now in the order $\bar{U}\bar{J}\bar{S}\bar{N}$) and henceforth secularly evolves with well-defined and periodic oscillations.

A second example of a repacked system, but one which becomes unstable, is illustrated in the right panel of Fig. 5 ($\bar{U}\bar{J}\bar{J}\bar{J}$ from simulation #2-24 of Table A2). Here, the unpacking occurs on the LWD phase, the smallest-mass planet is engulfed, and the two closest \bar{J} planets switch places.

3.2.5 Unpacked giant planets with test particles

In reality, the above systems likely harbour Mars-like planets or asteroids in regions like our Solar system’s asteroid belt. Simulation #11-19 ($\bar{J}\bar{U}\bar{N}\bar{S}$ and $\beta = 9$ from Table A11) contains 12 test particles located in initially circular orbits at 2.5 au. Figure 6 shows the resulting evolution. The four giant planets remain packed and stable through the entire simulation, and have a nondisruptive effect on the test particles during the main sequence and giant branch phases of evolution. However, on the white dwarf phase, eight of the 12 particles are lost. Seven are lost through ejections, all of which can be individually discerned on the plot (at times 6.22, 7.49, 7.71, 8.20, 10.08, 10.66 and 12.19 Gyr). One particle is engulfed inside of the white dwarf (as indicated in the table) at 10.29 Gyr.

3.2.6 Deep radial incursions for almost equal-mass planets

Tables A12 and A13 give details of simulations which contain almost equal-mass planets, and therefore serve as a useful basis of comparison to both other simulations in this work and previous simulations of strictly equal-mass planets. The mass ratios of consecutive planet pairs in the tables are just 3.34 and 1.18, respectively.

In Fig. 7, we display four simulations which show examples of how small ranges in planet mass within the same system can lead to deep radial incursions during the white dwarf phase. Shown are four-, six- and eight-planet systems. In three of the cases (simulations #12-8, #12-21 and #13-12) the runs did not finish. Unpacking occurs on the WD

phase in all cases, and instability results. The effects of tides (not modelled) might affect the green planets (which achieve pericentres of $\lesssim 0.1$ au) on the bottom plots.

3.3 The variety of system behaviours

Having illustrated some specific examples, now we consider the simulations in aggregate. Before inferring trends from the data, we first consider the rich variety of behaviours and outcomes seen in the simulations and simply list what is possible from full-lifetime evolution for clarity.

- Unpacking (defined as crossing orbits or planet loss) may occur during any phase of stellar evolution, or not at all.
- Unpacking through crossing orbits does not necessarily lead to instability (defined as planet loss from collisions or ejections)
 - Unpacking during one phase can lead to instability at a later phase.
 - Planet engulfment into the star, planet-planet collisions and ejections may all occur during any phase.
 - Two systems with identical initial numbers, masses and separations of planets can be unpacked at different phases and lose different numbers of planets.
 - Any total number of planets may be lost.
 - Planets which are formed when the star arrives on the main sequence at distances well outside of the maximum asymptotic giant branch stellar radius can be perturbed on the white dwarf phase to distances well within the maximum asymptotic giant branch stellar radius.
 - Test particles which initially reside within the orbits of four giant planets can survive for the entire simulation duration even when the giant planets unpack and/or become unstable.

3.4 General trends

In this section we present the crux of our results and some trends with applications beyond this work.

3.4.1 Relating to β

• Unpacking tends to occur at later stellar phases as β is increased. This correlation is typically strong but by no means monotonic. For example, consider simulations #8-1 through #8-32 (Table A8), where β is increased from 6.0 to 9.5. For a weaker correlation, instead see simulations #9-1 through #9-32 (Table A9), and for a better correlation, see simulations #4-1 through #4-24 (Table A4). See Fig. 8 for a visual representation of the correlation (although the tables themselves might be clearer).

• Mapping a particular value of β to the phase at which one could expect unpacking is architecture-dependent. Compare for example, the simulations with $\beta = 7.0$ across all of the tables.

• Terrestrial-mass planets (effectively, \bar{J} , \bar{S} , \bar{U} , and \bar{N}) at a given β will unpack at an earlier phase than their giant-planet counterparts (implied from Tables A1-A11 and Fig. 8) due to the additional dependence of stability timescale on mass, which is not captured by the Hill radius (e.g.

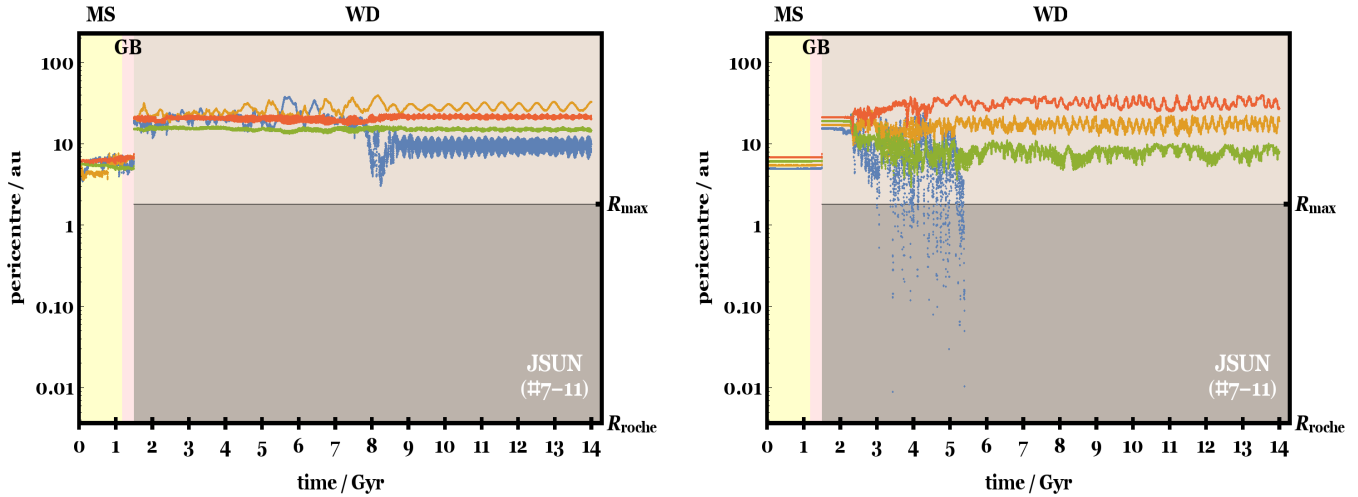


Figure 5. Two examples of unpacking then repacking, in both stable (left panel) and unstable (right panel) cases. *Left Panel:* Immediate unpacking of a set of terrestrial planets, followed by a re-ordering and stable secular evolution from 8 Gyr onwards. The initial order of the planets is $\bar{0}\bar{1}\bar{2}\bar{3}$ but their orbits end up in the order $\bar{0}\bar{3}\bar{2}\bar{1}$. Shown is simulation #9-39 (Table A9). *Right Panel:* Unpacking of $\bar{0}\bar{1}\bar{2}\bar{3}$ on the WD phase, where the least massive, innermost, planet becomes engulfed and two of the other planets (orange and green) switch order. Shown is simulation #2-24 (Table A2).

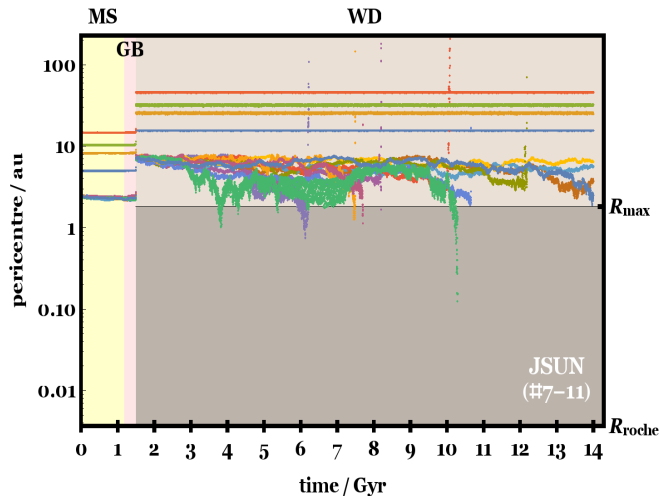


Figure 6. A stable and unpacked set of giant planets JUNS with 12 test particles initially located at 2.5 au. Four particles survive, seven are ejected, and one enters the white dwarf disruption radius at 10.29 Gyr. All these events are visible on the plot. Shown is simulation #11-19 (Table A11).

Chambers et al. 1996; Faber & Quillen 2007; Mustill et al. 2014).

3.4.2 Relating to engulfments, ejections and collisions

• Instability manifests itself primarily through ejections for giant planet systems and primarily through planet-planet collisions for terrestrial-planet systems. The two stark exceptions are the architectures $\bar{0}\bar{1}\bar{2}\bar{3}$ and $\bar{1}\bar{2}\bar{3}\bar{0}$ (Tables A2 and A1, where the lowest-mass terrestrial planet is engulfed into the white dwarf in the majority of cases (see e.g. Fig. 5).

- In-between these two regimes (giant planets and terrestrial planets) are the low-mass giant planets, or ice giants, with UNUN, UNUNUN and UNUNUNUN (Table A13). Only for these systems do unstable events appear to be roughly evenly distributed amongst ejections, engulfments and planet-planet collisions. For simulations #13-12 to #13-17, the lack of planet-planet collisions might be due to the truncated duration of those simulations and/or neglecting white dwarf-planet tides.

- Physically, the trends in the above two bullet points are understandable in terms of the Safronov number (Safronov & Zvjagina 1969), which is the square of the ratio of the surface escape speeds to the planetary orbital speeds. As this ratio increases, the frequency of ejections increases. This ratio is approximately unity for Earth-like planets at 20 au, but about 40 for Jupiters at the same separation.

- The commonality of planet-planet collisions in terrestrial planet systems implies that those systems should contain more debris and newly-generated asteroids than giant planet systems.

- The unpacking of systems with four giant planets preferentially (80%) results in the survival of two planets. This percentage would be 90% if not for the UNJS and NUJS architectures (Tables A9 and A10), which do not follow this trend. In these architectures, either the Uranus or Neptune is typically ejected but the other survives.

- The unpacking of systems with four terrestrial planets instead preferentially (55%) results in the survival of three planets, and in 30% of cases retains all four planets. This stark difference from the giant-planet case is likely related to the inability for close encounters in terrestrial-planet systems to be strong enough to cause ejections.

- Unpacked terrestrial-planet architectures which retain all planets are typically aperiodic in their resulting orbital variations (see e.g. Fig. 4). This feature is particularly noteworthy because these systems produce an ever-changing dy-

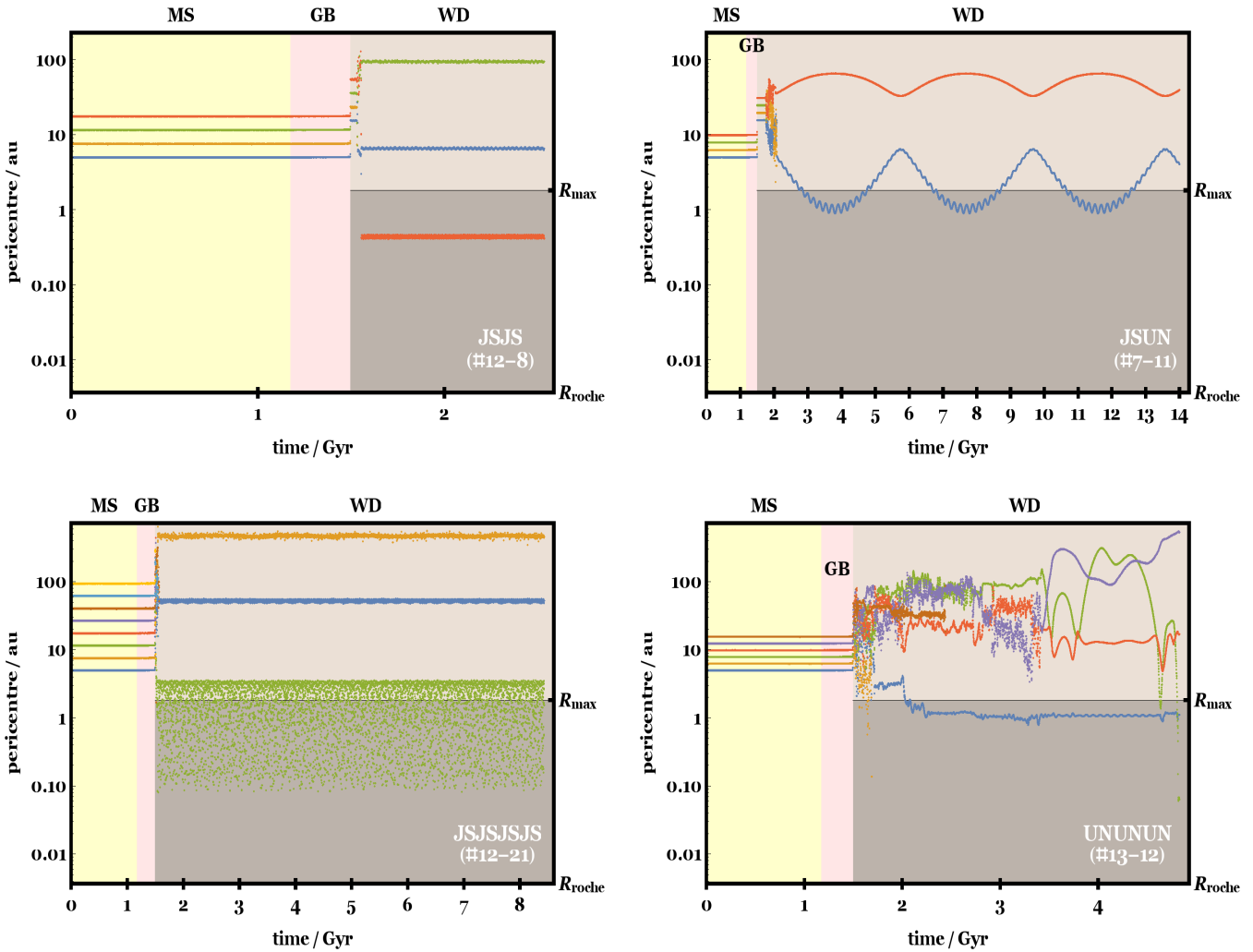


Figure 7. Deep radial incursions due to unpacking on the white dwarf phase of similar-mass giant planets in the systems JSJS (upper left panel, simulation #12-8), JSJSJSJS (lower left panel, simulation #12-21), UNUN (upper right panel, simulation #13-5) and UNUNUN (lower right panel, simulation #13-12). Tides are unlikely to play a role in the upper panels, but might affect the evolution of the green planets in the lower panels. The striking behaviour seen here is characteristic of the simulations from Tables A12 and A13.

namic environment, which may tap into different reservoirs of white dwarf pollutants at different cooling ages.

- When architectures contain one most massive planet (as opposed to two or more), as in Tables A1, A4, A7, A8, A9, A10 and A11, that planet is *never* ejected nor engulfed into the star. Physically, the reason is due to conservation of angular momentum and energy, even though the system energy is strictly not conserved during GB mass loss.

- For systems that contain exactly two most massive planets, those planets rarely are ejected or engulfed into the star. This tendency holds true for every single system simulated with Jupiters, Uranuses and their scaled equivalents JUJ, JÜÜJ, UJJU, ÜJJÜ (Tables A5 and A6). For JSJS (Table A12), where the difference in planet mass is much less (ratio of 3 as opposed to 22), there is only one exception (simulation #12-6). For UNUN (Table A13), there are two exceptions.

- Rarely (6.6%) does unpacking of four-planet systems allow for at least one of the planets to eventually achieve an or-

bital pericentre within the maximum AGB radius of 1.8 au, in contrast to the equal planet-mass case Veras & Gänsicke (2015).

- Deep radial incursions are most common for the unequal-mass systems which are closest to the equal-mass case, namely the UJJJ, ÜJJJ, JJJU, JJJÜ, JSJS and UNUN cases (Tables A2, A3, A12 and A13). The reason for the similarity is in the first four cases when one ignores/ejects the Uranus, and in the latter two cases because the range of their masses is small. In that respect, the greatest incidence of inward radial incursions occurs for the UNUN architecture, because with a mass ratio of 1.18 between adjacent pairs of planets, the system effectively contains equal-mass planets.

- Increasing the number of planets in a system increases the incidence for deep inward radial incursions, as well as consistently changing dynamical architectures, similar to the equal-planet mass case.

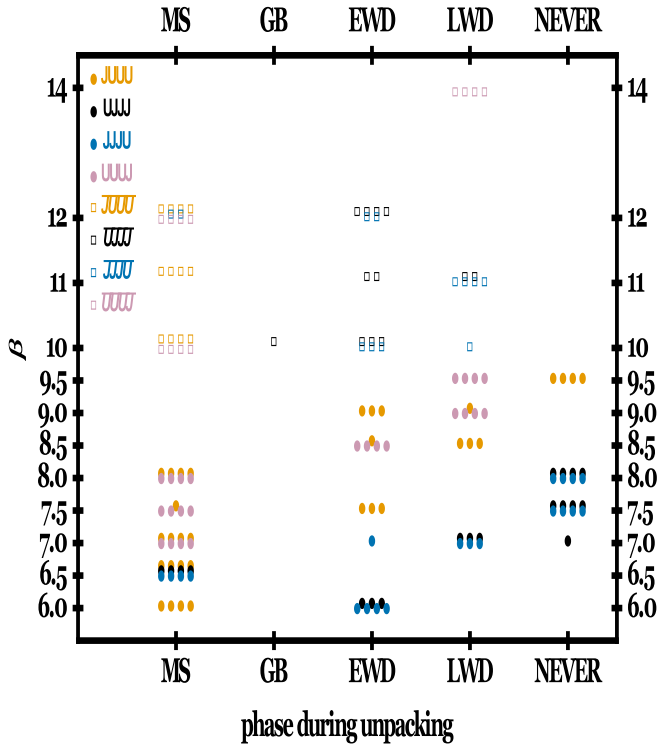


Figure 8. The phases at which unpacking occurs with respect to β for the eight architectures given in the legend. Each point represents one simulation. Generally, as β is increased, unpacking occurs during later phases, although the relationship is not monotonic. The terrestrial-sized planets (open squares) generally require higher values of β than giant planets (dots) to achieve the same results. Unpacking during the giant branch is rare.

3.4.3 Relating to test particles

- Unpacking of the non-zero mass planets enhances prospects for white dwarf engulfment of test particles, which can reasonably represent Mars-like planets or large asteroids.
- Even with the tiny sample sizes adopted here (12 test particles per simulation, as constrained by computational limitations), enough are engulfed by white dwarfs (263 out of a total 1024) to suggest both that this process is crucial and that higher resolution studies are needed to detect discernable trends.

4 DISCUSSION

In order to place our results in context, we will discuss the consequences for polluted white dwarf systems and consider the links to three outstanding observational constraints: (i) pollution rate with white dwarf cooling age, (ii) accumulated metal pollution in non-DA white dwarfs, and (iii) the WD 1145+017 system. We will also discuss the implications of so many ejections for the purported free-floating population of planets within the Milky Way, and how are simulations may be linked to chaos.

4.1 Consequences for polluted white dwarf systems

Our simulations clearly demonstrate that planet engulfment into white dwarfs is a rare phenomenon (8.8% across all simulations), in line with the findings of the equal-planet mass studies of Veras et al. (2013a), Mustill et al. (2014) and Veras & Gänsicke (2015). A much more likely pollution reservoir is the test particles, which we have shown can easily be engulfed in the white dwarf, in line with the one-planet studies of Bonsor et al. (2011), Debes et al. (2012) and Frewen & Hansen (2014). The difference here is that multiple planets provide the opportunity for a constantly changing dynamic environment, which is not the case in one-planet systems⁶. Consequently, multiple-planet systems are much more likely to explain high rates of pollution at different cooling ages by accessing and perturbing different reservoirs of material (asteroids, fragments, dust) at different times and/or different locations.

Here we have characterized this environment by sampling systems of unequal-mass planets, where the planet masses differ by a factor of up to about 20. We found that this inequality has clear but second-order effects on the dynamics; the first-order effects are determined by what types of planets are involved in the unpacking: terrestrial or giant. For giant planets, crossing orbits trigger violent encounters between giant planets, but still typically cause the system to settle into a periodic secular state (see Fig. 2 and the upper-left panel of Fig. 7). For terrestrial planets, fully 30% of our simulations become unpacked (orbit-crossed) but never unstable (featuring engulfments, ejections or collisions). The result is a highly dynamic environment, where the planetary orbits meander (see Fig. 4), which is much more conducive to effective scattering at late ages.

4.2 Correlation with cooling age

Our choice of dividing up the white dwarf phase into separate EWD and LWD phases was partly motivated by our simulation results, because a white dwarf cooling age of 100 Myr is a representative end value for the epoch of rapid post-main-sequence planetary instability (see e.g. Fig. 9). However, this value is also sensible from an observational point-of-view. The cooling ages of the white dwarfs in Koester et al. (2014) are all below 200 Myr, while white dwarf atmospheric properties can significantly change at cooling ages of ~ 500 Myr (see their Fig. 8, middle panel). Therefore, a cut at cooling ages of a few 100 Myr is a natural way to separate samples observationally.

However, observations obtained so far indicate that the accretion rate of metals onto white dwarf atmospheres remains a flat function of white dwarf cooling age (Fig. 4 of Koester et al. 2014). Explaining pollution at late times (after many Gyr of white dwarf evolution) is challenging because instability on the white dwarf phase is partially triggered by the increase in system stochasticity due to

⁶ Stellar flybys can change the environment regardless of the number of planets, but typically 10 Gyr needs to pass before a flyby achieves a close encounter within a few hundred au (Zakamska & Tremaine 2004; Veras & Moeckel 2012).

RGB and AGB mass loss (Voyatzis et al. 2013), preferentially leading to instabilities at early cooling ages. Fig. 9 emphasizes this tendency, even though this study does not attempt to model a realistic population synthesis (which is anyway beyond current computational means).

Recent and ongoing work is exploring potential ways of polluting white dwarfs at late cooling ages. One possibility is through the change in orbits of wide binary stellar companions due to Galactic tides after, and only after, one of the components has become a white dwarf (Bonsor & Veras 2015). However, the majority of known polluted white dwarfs do not appear to harbour wide-orbit companions. Another possibility is through Lidov-Kozai secular evolution amongst multiple planets, such that the close encounters between planets and white dwarfs first occur only after cooling ages of several Gyr (C. Petrovich & D. Muñoz, in preparation). Finally, an extant fragment field from planet-planet collisions may persist for several Gyr before being thrust towards the white dwarf (A. Shannon et al., in preparation).

For the architectures we have explored here, there is a similar spike in instabilities just after mass loss from the tip of the AGB during the EWS phase. However, planetary systems which remain stable through that epoch exhibit a wide range of instability times, and instances when a planet or test particle approaches the vicinity of the white dwarf. Meandering of low-mass (terrestrial-like) planets provides a dynamic environment with which extant debris or fragments may be perturbed to the white dwarfs at all ages. Our results show that mass equality amongst planets is not a requirement for late-age pollution, and is not in fact even preferential for producing instabilities at late ages.

4.3 Accumulated metals in convection zone

White dwarfs with deep convection zones (usually containing Helium-dominated atmospheres) retain a measurable record of the accreted planetary debris over a span of time up to a few Myr (see Fig. 1 of Wyatt et al. 2014). Fig. 6 of Veras (2016) illustrates the amount of mass accreted for three different samples from Farihi et al. (2010), Girven et al. (2012) and Xu & Jura (2012).

The accumulated mass ranges from the mass of Phobos to that of Pluto, and may have been accrued by a single object or a collection of bodies. Distinguishing these two possibilities is not possible observationally. From theory, we may determine the likelihood of a sequence of bodies impacting the white dwarf or entering its Roche radius within 1 Myr. However, the sample size of the test particles in our simulations here (12 per simulation) was too small to determine impact frequency for a given architecture.

The accretion itself might represent a combination of a “continuous” stream of small particles from a surrounding disc and a “stochastic” agglomeration of larger particles from elsewhere in the system. Wyatt et al. (2014) showed that the size boundary between these two regimes is approximately 35 km, and further constrained the potential size distribution of this accreted material, ruling out a mono-mass distribution. Further, discs have been detected around only a few percent of polluted white dwarfs (Farihi et al. 2009; Girven et al. 2011; Steele et al. 2011), although the actual fraction is likely greater than half (Bergfors et al.

2014). Consequently, stochastic accretion is likely to play a role in many of these systems. The mechanics of impact into white dwarf atmospheres indicates that the parameter space may be split into sublimation, fragmentation and ablation regimes (J. C. Brown et al., in preparation) such that the details of the deposition are complex, but the end result is still metals in the convection zone.

4.4 WD 1145+017

The WD 1145+017 planetary system represents the only example of a metal-polluted white dwarf with a surrounding debris disc composed of both dust and gas and disintegrating objects (asteroids, planets, or something in-between) detected by transit photometry. In this respect, the system provides a self-consistent snapshot of the disc formation and accretion process that is likely to take place at other metal-polluted white dwarfs, and confirms long-standing theories (Graham et al. 1990; Jura 2003; Bear & Soker 2013).

The system was announced by Vanderburg et al. (2015), who presented transit curves that illustrated that up to six objects with orbital periods of about 4.5–4.9 hours are in the process of disintegrating and producing dust. They found that the dominant orbital period is closer to 4.5 hours, which places the objects near the white dwarf’s Roche radius, assuming that the objects are rubble-piles like the asteroids seen in the Solar system. The size of these objects are poorly constrained, and could range anywhere from ~ 1 to 1000 km. We will henceforth refer to them as planetesimals.

Follow-up observations came quickly (Croll et al. 2016; Gänsicke et al. 2016; Rappaport et al. 2016; Xu et al. 2016). Xu et al. (2016) detected gas in the debris disc and showed that the white dwarf atmosphere is polluted with 11 heavy elements. Croll et al. (2016) performed multi-wavelength observations that illustrated the number of planetesimals disintegrating is likely more than one, and helped confirm that the planetesimals harbour an orbital period of about 4.5 hours rather than a value closer to 4.9 hours. Further follow-up was provided by Gänsicke et al. (2016), who used high-speed photometry and observations of the system from Nov-Dec 2015 to reveal that at least six planetesimals are breaking up, and that they share the same near-circular orbit with orbital periods of about 4.4930 hours. Rappaport et al. (2016) most recently detected drifting features which they postulate are fragments that broke off from a single progenitor.

Our results, along with those of Bonsor et al. (2011), Debes et al. (2012), Frewen & Hansen (2014) and Veras & Gänsicke (2015), demonstrate that the progenitor of the planetesimals in WD 1145+017 may be a large asteroid that was scattered in the vicinity of the WD. The scattering may be caused by one planet (Bonsor et al. 2011; Debes et al. 2012; Frewen & Hansen 2014) or multiple planets (this paper). Alternatively, the progenitor may be a moon (Payne et al. 2016), or a small (terrestrial) planet, as shown by both Veras & Gänsicke (2015) and this paper. Multiple planets can scatter a test particle into a transit-detectable orbit, even if the planets themselves never unpack (Fig. 6). We note that a Solar system analogue, with JSUN and asteroids or a Mars, can easily generate the progenitor of the planetesimals in WD 1145+017. The mass of the progenitor remains unconstrained (Veras et al. 2016).

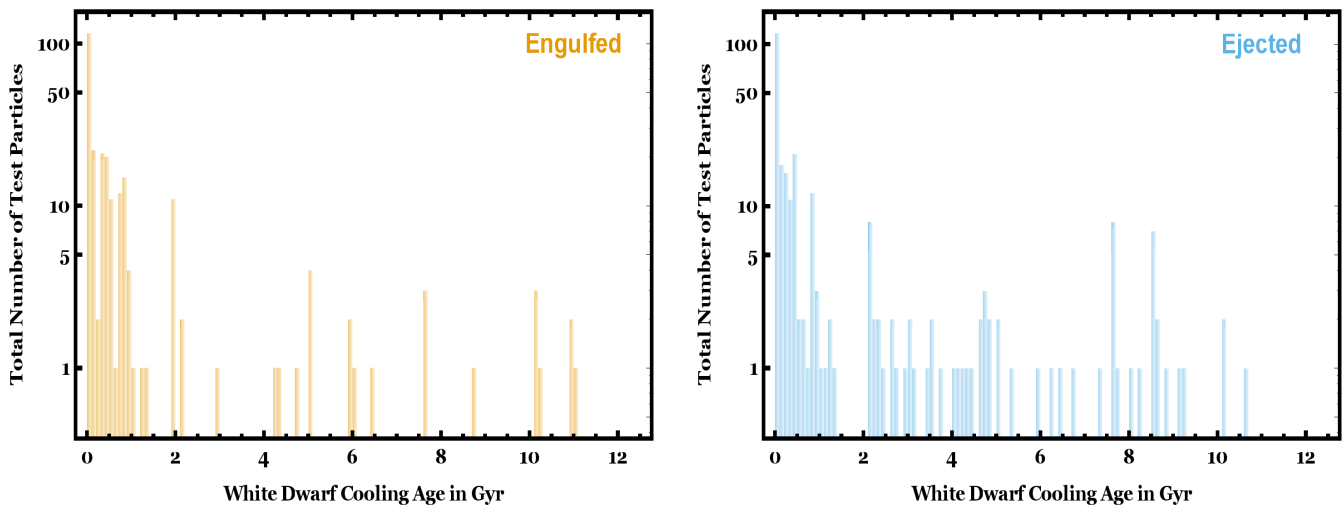


Figure 9. The white dwarf cooling age (time since becoming a white dwarf) at which test particles across all simulations entered the white dwarf Roche radius (*left panel*) or were ejected from the system (*right panel*). The EWD phase corresponds to the first bin, and the LWD phase to all other bins. The histograms illustrate the pollution decay rate obtained from the simulations.

Our simulations suggest that WD 1145+017 is not unique in hosting transiting planetesimals. Many possible multi-planet scenarios can perturb test particles into the Roche radius of the white dwarf; we have just scratched the surface.

4.5 Free-floating planet population contribution

A brief inspection of the tables in the appendix reveal a preponderance of planetary ejections. This feature, just like for the equal-mass planet case (Veras et al. 2013a; Mustill et al. 2014), and even the single-planet case (Veras et al. 2011; Veras & Tout 2012; Veras et al. 2014c), help establish that planetary ejection is an ubiquitous feature of post-main-sequence systems. Consequently, these ejections make a contribution to the free-floating planet population.

How this contribution compares to that due to the dynamical activity which accompanies planetary formation and protoplanetary disc dissipation (e.g. Rasio & Ford 1996; Levison et al. 1998; Marzari & Weidenschilling 2002; Veras & Armitage 2005, 2006; Raymond et al. 2011, 2012; Matsumura et al. 2013) is not yet clear, primarily because our observational knowledge of exoplanets beyond 5 au is sparse. Nevertheless, we have an extraordinary observational estimate on the total number of free-floating giant planets in the Milky Way: nearly two for every main sequence star (Sumi et al. 2011). If future observations affirm this result, then a major question in planetary science will remain identifying the origin of so many free-floaters. Planetary scattering alone with single stars on the main sequence cannot explain this population (Veras & Raymond 2012), and the contribution from scattering in binary systems has not yet been quantified, despite studies such as Sutherland & Fabrycky (2015) and Smullen et al. (2016).

We caution that although ejections were perhaps common amongst the currently observed population of white dwarfs (as illustrated by this study), the resulting contribution to the currently observed free-floating planet pop-

ulation as reported by Sumi et al. (2011) would be on the order of 1% (Veras & Raymond 2012). Each white dwarf progenitor system would need to have harboured tens of *giant* planets to achieve the Sumi et al. (2011) result. This number is thought to be too large, despite the likely positive correlation between stellar mass and planet multiplicity (Kennedy & Kenyon 2008; Andrews et al. 2013), partly because of the extreme case HR 8799, which contains (just) four giant and packed planets (Marois et al. 2010). HR 8799 also provides a representative glimpse into the past of white dwarf planetary systems because of its A-star host.

4.6 Linking meandering with chaotic behaviour

The phenomenon we refer to as meandering is linked to the stochasticity of the system. The vast literature on chaos indicators in gravitational point-mass exoplanetary systems utilizes a wide variety of techniques in order to characterize, in part, how close the system is to instability at different times. Linking these indicators to N -body integrations – particularly long-term integrations – remains challenging (e.g. Veras, Antoniadou & Gänsicke, In Prep) but may provide key constraints.

Only two published dedicated post-main-sequence studies of which we are aware have attempted to link evolution with stochasticity at the beginning and end of mass loss (Adams et al. 2013; Voyatzis et al. 2013). Both studies use the classical Lyapunov exponent as their chaos indicators, and consider two planets. Their work brings attention to subtleties which indicate that dedicated studies on chaos would be beneficial. We frame these subtleties as the following questions: (i) What metric (e.g. Cartesian coordinate, eccentricity), and corresponding reference frame or coordinate system, would provide the most representative link to instability?, (ii) How does one combine chaos indicators for multi-planet systems, particularly after close encounters, and after one or more of the planets is lost from the system?, (iii) What chaos indicators are affected by the Hamiltonian-

breaking physics of stellar mass loss, and how do different mass loss prescriptions affect the usefulness of a particular indicator?

Although these questions are too big to tackle here, our simulations provide a template on which future dedicated studies may make useful comparisons.

5 CONCLUSIONS

We have performed over 450 full-lifetime simulations of unequal-mass planets, which finally removes the long-standing equal-mass constraint from previous studies. We have also for the first time simulated the post-main-sequence evolution of multiple planets with test particles. Appendix A displays the results and characteristics of all simulations. The trends in the data are outlined in bulleted form in Section 3.4, and are summarized here as

- Unlike in the giant planet case, terrestrial-planet unpacking (orbit crossing) often does not trigger instability (engulfments, ejections and collisions), and provides a more dynamic, constantly shifting evolution throughout the white dwarf phase; this result is independent of the mass variation amongst planets.

- The smaller the dispersion in planetary mass, the closer those planets may be perturbed towards the white dwarf.

- Giant planet systems preferentially feature ejections whereas terrestrial-planet systems preferentially feature planet-planet collisions. Consequently, we expect more potentially polluting debris to exist in terrestrial-planet systems.

- Prospects for unpacking roughly increase as β increases, although this relationship is not-monotonic and dependent on the considered architecture.

Ultimately, how planets behave at different phases of evolution will crucially determine the subsequent evolution of the smaller bodies in those systems, bodies which are most likely the progenitors of white dwarf pollution and planetesimals such as those observed disintegrating around WD 1145+017.

ACKNOWLEDGEMENTS

DV and BTG have received funding from the European Research Council under the European Union's Seventh Framework Programme (FP/2007-2013)/ERC Grant Agreement n. 320964 (WDTracer). AJM acknowledges support from grant number KAW 2012.0150 from the Knut and Alice Wallenberg foundation and the Swedish Research Council (grant 2011-3991).

REFERENCES

Adams, F. C., Anderson, K. R., & Bloch, A. M. 2013, MNRAS, 432, 438
 Andrews, S. M., Rosenfeld, K. A., Kraus, A. L., & Wilner, D. J. 2013, ApJ, 771, 129
 Barclay, T., Quintana, E. V., Adams, F. C., et al. 2015, ApJ, 809, 7
 Bear, E., & Soker, N. 2013, New Astronomy, 19, 56

Bergfors, C., Farihi, J., Dufour, P., & Rocchetto, M. 2014, MNRAS, 444, 2147
 Bonsor, A., Mustill, A. J., & Wyatt, M. C. 2011, MNRAS, 414, 930
 Bonsor, A., & Veras, D. 2015, MNRAS, 454, 53
 Campante, T. L., Barclay, T., Swift, J. J., et al. 2015, ApJ, 799, 170
 Casewell, S. L., Dobbie, P. D., Napiwotzki, R., et al. 2009, MNRAS, 395, 1795
 Cassan, A., Kubas, D., Beaulieu, J.-P., et al. 2012, Nature, 481, 167
 Catalán, S., Isern, J., García-Berro, E., & Ribas, I. 2008, MNRAS, 387, 1693
 Chambers, J. E., Wetherill, G. W., & Boss, A. P. 1996, Icarus, 119, 261
 Chambers, J. E. 1999, MNRAS, 304, 793
 Croll, B., Dalba, P. A., Vanderburg, A., et al. 2016, Submitted to ApJL, arXiv:1510.06434
 Davies, M. B., Adams, F. C., Armitage, P., et al. 2014, Protostars and Planets VI, 787
 Debes, J. H., & Sigurdsson, S. 2002, ApJ, 572, 556
 Debes, J. H., Walsh, K. J., & Stark, C. 2012, ApJ, 747, 148
 Dong, R., Wang, Y., Lin, D. N. C., & Liu, X.-W. 2010, ApJ, 715, 1036
 Dufour, P., Bergeron, P., Liebert, J., et al. 2007, ApJ, 663, 1291
 Duncan, M. J., & Lissauer, J. J. 1998, Icarus, 134, 303
 Faber, P., & Quillen, A. C. 2007, MNRAS, 382, 1823
 Falcon, R. E., Winget, D. E., Montgomery, M. H., & Williams, K. A. 2010, ApJ, 712, 585
 Farihi, J., Jura, M., & Zuckerman, B. 2009, ApJ, 694, 805
 Farihi, J., Barstow, M. A., Redfield, S., Dufour, P., & Hambly, N. C. 2010, MNRAS, 404, 2123
 Farihi, J. 2016 Submitted, New Astronomy Reviews.
 Frewen, S. F. N., & Hansen, B. M. S. 2014, MNRAS, 439, 2442
 Gänsicke, B. T., Aungwerojwit, A., Marsh, T. R. et al. 2016, In Press ApJL, arXiv:1512.09150
 Gentile Fusillo, N. P., Gänsicke, B. T., & Greiss, S. 2015, MNRAS, 448, 2260
 Girven, J., Gänsicke, B. T., Steeghs, D., & Koester, D. 2011, MNRAS, 417, 1210
 Girven, J., Brinkworth, C. S., Farihi, J., et al. 2012, ApJ, 749, 154
 Gomes, R., Levison, H. F., Tsiganis, K., & Morbidelli, A. 2005, Nature, 435, 466
 Graham, J. R., Matthews, K., Neugebauer, G., & Soifer, B. T. 1990, ApJ, 357, 216
 Guillochon, J., Ramirez-Ruiz, E., & Lin, D. 2011, ApJ, 732, 74
 Henning, W. G., & Hurford, T. 2014, ApJ, 789, 30
 Hurley, J. R., Pols, O. R., & Tout, C. A. 2000, MNRAS, 315, 543
 Izidoro, A., Raymond, S. N., Morbidelli, A., & Winter, O. C. 2015, MNRAS, 453, 3619
 Jura, M. 2003, ApJL, 584, L91
 Kalirai, J. S., Hansen, B. M. S., Kelson, D. D., et al. 2008, ApJ, 676, 594
 Kennedy, G. M., & Kenyon, S. J. 2008, ApJ, 673, 502
 Kepler, S. O., Pelisoli, I., Koester, D., et al. 2015, MNRAS, 446, 4078
 Kepler, S. O., Pelisoli, I., Koester, D., et al. 2016, MNRAS,

- 455, 3413
- Kleinman, S. J., Kepler, S. O., Koester, D., et al. 2013, *ApJS*, 204, 5
- Koester, D., Gänsicke, B. T., & Farihi, J. 2014, *A&A*, 566, A34
- Levison, H. F., Lissauer, J. J., & Duncan, M. J. 1998, *AJ*, 116, 1998
- Levison, H. F., Morbidelli, A., Tsiganis, K., Nesvorný, D., & Gomes, R. 2011, *AJ*, 142, 152
- Liebert, J., Bergeron, P., & Holberg, J. B. 2005, *ApJS*, 156, 47
- Liu, S.-F., Guillochon, J., Lin, D. N. C., & Ramirez-Ruiz, E. 2013, *ApJ*, 762, 37
- Luhman, K. L., Burgasser, A. J., & Bochanski, J. J. 2011, *ApJL*, 730, L9
- Marois, C., Zuckerman, B., Konopacky, Q. M., Macintosh, B., & Barman, T. 2010, *Nature*, 468, 1080
- Marzari, F., & Weidenschilling, S. J. 2002, *Icarus*, 156, 570
- Matsumura, S., Ida, S., & Nagasawa, M. 2013, *ApJ*, 767, 129
- Morbidelli, A., Levison, H. F., Tsiganis, K., & Gomes, R. 2005, *Nature*, 435, 462
- Mustill, A. J., & Villaver, E. 2012, *ApJ*, 761, 121
- Mustill, A. J., Marshall, J. P., Villaver, E., et al. 2013, *MNRAS*, 436, 2515
- Mustill, A. J., Veras, D., & Villaver, E. 2014, *MNRAS*, 437, 1404
- Nordhaus, J., & Spiegel, D. S. 2013, *MNRAS*, 432, 500
- O'Brien, D. P., Walsh, K. J., Morbidelli, A., Raymond, S. N., & Mandell, A. M. 2014, *Icarus*, 239, 74
- Paxton, B., Bildsten, L., Dotter, A., et al. 2011, *ApJS*, 192, 3
- Paxton, B., Marchant, P., Schwab, J., et al. 2015, *ApJS*, 220, 15
- Payne, M. J., Veras, D., Holman, M. J., et al. 2016, *MNRAS*, 457, 217
- Pierens, A., & Raymond, S. N. 2011, *A&A*, 533, A131
- Portegies Zwart, S. 2013, *MNRAS*, 429, L45
- Pu, B., & Wu, Y. 2015, *ApJ*, 807, 44
- Rappaport, S., Gary, B. L., Kaye, T., et al. 2016, Submitted to *MNRAS*, arXiv:1602.00740
- Rasio, F. A., & Ford, E. B. 1996, *Science*, 274, 954
- Raymond, S. N., Armitage, P. J., Moro-Martín, A., et al. 2011, *A&A*, 530, A62
- Raymond, S. N., Armitage, P. J., Moro-Martín, A., et al. 2012, *A&A*, 541, A11
- Reffert, S., Bergmann, C., Quirrenbach, A., Trifonov, T., Künstler, A. 2015, *A&A*, 574, A116
- Safronov, V. S., & Zvjagina, E. V. 1969, *Icarus*, 10, 109
- Schröder, K.-P., & Connors, R. 2008, *MNRAS*, 386, 155
- Schröder, K.-P., & Cuntz, M. 2005, *ApJL*, 630, L73
- Sigurdsson, S., Richer, H. B., Hansen, B. M., Stairs, I. H., & Thorsett, S. E. 2003, *Science*, 301, 193
- Smith, A. W., & Lissauer, J. J. 2009, *Icarus*, 201, 381
- Smullen, R. A., Kratter, K. M., Shannon, A. 2016, Submitted to *ApJ*
- Steele, P. R., Burleigh, M. R., Dobbie, P. D., et al. 2011, *MNRAS*, 416, 2768
- Sumi, T., Kamiya, K., Bennett, D. P., et al. 2011, *Nature*, 473, 349
- Sutherland, A. P., & Fabrycky, D. C. 2015, Submitted to *ApJ*, arXiv:1511.03274
- Tremblay, P.-E., Ludwig, H.-G., Steffen, M., & Freytag, B. 2013, *A&A*, 559, A104
- Tsiganis, K., Gomes, R., Morbidelli, A., & Levison, H. F. 2005, *Nature*, 435, 459
- Vanderburg, A., Johnson, J. A., Rappaport, S., et al. 2015, *Nature*, 526, 546
- Veras, D., & Armitage, P. J. 2005, *ApJL*, 620, L111
- Veras, D., & Armitage, P. J. 2006, *ApJ*, 645, 1509
- Veras, D., & Ford, E. B. 2010, *ApJ*, 715, 803
- Veras, D., Wyatt, M. C., Mustill, A. J., Bonsor, A., & Eldridge, J. J. 2011, *MNRAS*, 417, 2104
- Veras, D., & Moeckel, N. 2012, *MNRAS*, 425, 680
- Veras, D., & Raymond, S. N. 2012, *MNRAS*, 421, L117
- Veras, D., & Tout, C. A. 2012, *MNRAS*, 422, 1648
- Veras, D., & Evans, N. W. 2013, *MNRAS*, 430, 803
- Veras, D., Mustill, A. J., Bonsor, A., & Wyatt, M. C. 2013a, *MNRAS*, 431, 1686
- Veras, D., Hadjidemetriou, J. D., & Tout, C. A. 2013b, *MNRAS*, 435, 2416
- Veras, D., Jacobson, S. A., Gänsicke, B. T. 2014a, *MNRAS*, 445, 2794
- Veras, D., Shannon, A., Gänsicke, B. T. 2014b, *MNRAS*, 445, 4175
- Veras, D., Evans, N. W., Wyatt, M. C., & Tout, C. A. 2014c, *MNRAS*, 437, 1127
- Veras, D., Leinhardt, Z. M., Bonsor, A., Gänsicke, B. T. 2014d, *MNRAS*, 445, 2244
- Veras, D., Eggl, S., Gänsicke, B. T. 2015a, *MNRAS*, 451, 2814
- Veras, D., Eggl, S., Gänsicke, B. T. 2015b, *MNRAS*, 452, 1945
- Veras, D., Gänsicke, B. T. 2015, *MNRAS*, 447, 1049
- Veras, D., 2016, *Royal Society Open Science*, 3:150571.
- Veras, D., Marsh, T. R., Gänsicke, B. T. 2016, Submitted to *MNRAS*
- Villaver, E., Livio, M., Mustill, A. J., & Siess, L. 2014, *ApJ*, 794, 3
- Voyatzis, G., Hadjidemetriou, J. D., Veras, D., & Varvoglis, H. 2013, *MNRAS*, 430, 3383
- Walsh, K. J., Morbidelli, A., Raymond, S. N., O'Brien, D. P., & Mandell, A. M. 2011, *Nature*, 475, 206
- Winn, J. N., & Fabrycky, D. C. 2015, *ARA&A*, 53, 409
- Wyatt, M. C., Farihi, J., Pringle, J. E., & Bonsor, A. 2014, *MNRAS*, 439, 3371
- Xu, S., & Jura, M. 2012, *ApJ*, 745, 88
- Xu, S., Jura, M., Dufour, P., & Zuckerman, B. 2016, In Press *ApJL*, arXiv:1511.05973
- Zakamska, N. L., & Tremaine, S. 2004, *AJ*, 128, 869
- Zuckerman, B., Koester, D., Reid, I. N., Hüensch, M. 2003, *ApJ*, 596, 477
- Zuckerman, B., Melis, C., Klein, B., Koester, D., & Jura, M. 2010, *ApJ*, 722, 725

APPENDIX A: SIMULATION DATA TABLES

In this appendix, we present characteristics of every simulation, one per row. The simulation sets are split into tables according to the masses and ordering of planets simulated. See Sec. 3.1 for a full description of the table columns.

Table A1. Summary of results for JUUU and J̄UŪ. We summarize the column definitions (see Sec. 3.1 for a full description) as: **Sim #**: Simulation designation. **Setup**: Planet type and order from closest to furthest. Overbars denote a mass reduction by a factor of 318. **β** : Number of mutual Hill radii. **Unpack**: Stellar phase during which unpacking occurs. **# Surv**: Number of surviving planets **Engulf**: Planets (identified in subscripts in number order from closest to furthest) which intersect the star's surface or Roche radius, and the phase when the engulfment occurs. **Eject**: Planets (identified in subscripts in number order from closest to furthest) which are ejected from the system, and the phase when the ejection occurs. **Collision**: Planets (identified in subscripts in number order from closest to furthest) which collide with one another, and the phase when the collision occurs. **$< R_{\max}$** : Surviving planets (identified in number order from closest to furthest) which achieve an orbital pericentre less than 1.82 au during the EWD or LWD phase; the minimum pericentre is provided in the subscript. **TPs Eng**: Number of test particles out of 12 which are engulfed in the EWD/LWD phases. **Phase abbreviations**: MS = main sequence, GB = giant branch, EWD = white dwarf with 0-100 Myr cooling, LWD = white dwarf beyond 100 Myr cooling.

Notes:

^dA test particle which survived the entire integration achieved a minimum pericentre of 0.062 au at a WD cooling age of 1.983 Gyr.

Sim #	Setup	β	Unpack	# Surv	Engulf	Eject	Collision	$< R_{\max}$?	TPs Eng	Notes
1-1	JUUU	6.0	MS	2		MS ₂ ,MS ₃				
1-2	JUUU	6.0	MS	2		MS ₃	MS ₁₋₂			
1-3	JUUU	6.0	MS	2		MS ₂ ,MS ₃				
1-4	JUUU	6.0	MS	2		MS ₂ ,MS ₃				
1-5	JUUU	6.5	MS	2		MS ₃ ,MS ₄				
1-6	JUUU	6.5	MS	2		MS ₃ ,MS ₄				
1-7	JUUU	6.5	MS	2		MS ₃	MS ₁₋₄			
1-8	JUUU	6.5	MS	2		MS ₂ ,MS ₃				
1-9	JUUU	7.0	MS	2		MS ₂ ,MS ₃				
1-10	JUUU	7.0	MS	2		MS ₂ ,MS ₃				
1-11	JUUU	7.0	MS	2		MS ₃ ,MS ₄				
1-12	JUUU	7.0	MS	2		MS ₂	MS ₃₋₄			
1-13	JUUU	7.5	MS	2		MS ₂ ,MS ₄				
1-14	JUUU	7.5	EWD	2		EWD ₃ ,EWD ₄				
1-15	JUUU	7.5	EWD	2		EWD ₃ ,EWD ₄				
1-16	JUUU	7.5	EWD	2		EWD ₂ ,EWD ₄				
1-17	JUUU	8.0	MS	2		MS ₃ ,EWD ₄				d
1-18	JUUU	8.0	MS	2		MS ₃ ,MS ₄				
1-19	JUUU	8.0	MS	2		MS ₂ ,MS ₃				
1-20	JUUU	8.0	MS	2		MS ₃ ,MS ₄				
1-21	JUUU	8.5	EWD	2		EWD ₃ ,EWD ₄			(0/0)	
1-22	JUUU	8.5	LWD	2		LWD ₂ ,LWD ₄			(0/0)	
1-23	JUUU	8.5	LWD	2		LWD ₂ ,LWD ₃			(0/4)	
1-24	JUUU	8.5	LWD	2		LWD ₂ ,LWD ₄			(0/0)	
1-25	JUUU	9.0	LWD	2		LWD ₂ ,LWD ₃			(0/0)	
1-26	JUUU	9.0	EWD	2		EWD ₃ ,EWD ₄			(0/0)	
1-27	JUUU	9.0	EWD	2		EWD ₃ ,EWD ₄			(3/2)	
1-28	JUUU	9.0	EWD	2		EWD ₃ ,EWD ₄			(2/0)	
1-29	JUUU	9.5		4					(0/0)	
1-30	JUUU	9.5		4					(0/0)	
1-31	JUUU	9.5		4					(0/0)	
1-32	JUUU	9.5		4					(0/0)	
1-33	J̄UŪ	10.0	MS	3			MS ₁₋₄			
1-34	J̄UŪ	10.0	MS	2			MS ₂₋₃ ,MS ₁₋₂			
1-35	J̄UŪ	10.0	MS	3			MS ₁₋₂			
1-36	J̄UŪ	10.0	MS	2			MS ₁₋₄ ,MS ₁₋₂			
1-37	J̄UŪ	11.0	MS	3			MS ₃₋₄			
1-38	J̄UŪ	11.0	MS	2			MS ₁₋₂ ,MS ₃₋₄			
1-39	J̄UŪ	11.0	MS	2			MS ₁₋₃ ,LWD ₁₋₂			
1-40	J̄UŪ	11.0	MS	4						
1-41	J̄UŪ	12.0	MS	2			MS ₁₋₃ ,LWD ₁₋₄			
1-42	J̄UŪ	12.0	MS	4						
1-43	J̄UŪ	12.0	MS	3		LWD ₃				
1-44	J̄UŪ	12.0	MS	3			MS ₁₋₂			

Table A2. Summary of results for UJJJ and $\bar{U}\bar{J}\bar{J}\bar{J}$. See Sec. 3.1 for a full description of the columns or Table A1 for a summary. MS = main sequence, GB = giant branch, EWD = white dwarf with 0-100 Myr cooling, LWD = white dwarf beyond 100 Myr cooling. Notes:

^aSubsequent evolution may have been affected by tides on the GB phase.

Sim #	Setup	β	Unpack	# Surv	Engulf	Eject	Collision	$< R_{\max}$?	TPs Eng	Notes
2-1	UJJJ	6.0	EWD	2		EWD ₃ ,EWD ₄		#2 _{1.449}		
2-2	UJJJ	6.0	EWD	2	EWD ₁	LWD ₂		#4 _{0.448}		
2-3	UJJJ	6.0	EWD	2		EWD ₁ ,EWD ₂				
2-4	UJJJ	6.5	MS	2	MS ₁	MS ₂				
2-5	UJJJ	6.5	MS	2		MS ₁ ,EWD ₄		#3 _{1.114}		
2-6	UJJJ	6.5	MS	2		MS ₁ ,LWD ₂				
2-7	UJJJ	6.5	MS	2		MS ₁	MS ₃₋₄			
2-8	UJJJ	7.0	LWD	2		LWD ₁ ,LWD ₃				
2-9	UJJJ	7.0		4						
2-10	UJJJ	7.0	LWD	2		LWD ₁ ,LWD ₃				
2-11	UJJJ	7.0	LWD	3		LWD ₁				
2-12	UJJJ	7.5		4						
2-13	UJJJ	7.5		4						
2-14	UJJJ	7.5		4						
2-15	UJJJ	7.5		4						
2-16	UJJJ	8.0		4						
2-17	UJJJ	8.0		4						
2-18	UJJJ	8.0		4						
2-19	UJJJ	8.0		4						
2-20	$\bar{U}\bar{J}\bar{J}\bar{J}$	10.0	EWD	3			EWD ₁₋₃	#2 _{0.833}		
2-21	$\bar{U}\bar{J}\bar{J}\bar{J}$	10.0	EWD	3	LWD ₁					
2-22	$\bar{U}\bar{J}\bar{J}\bar{J}$	10.0	EWD	3	LWD ₁					
2-23	$\bar{U}\bar{J}\bar{J}\bar{J}$	10.0	GB	3	LWD ₁					a
2-24	$\bar{U}\bar{J}\bar{J}\bar{J}$	11.0	LWD	3	LWD ₁					
2-25	$\bar{U}\bar{J}\bar{J}\bar{J}$	11.0	LWD	4				#4 _{0.989}		
2-26	$\bar{U}\bar{J}\bar{J}\bar{J}$	11.0	EWD	3	LWD ₁					
2-27	$\bar{U}\bar{J}\bar{J}\bar{J}$	11.0	EWD	3	LWD ₁					
2-28	$\bar{U}\bar{J}\bar{J}\bar{J}$	12.0	EWD	3	LWD ₁					
2-29	$\bar{U}\bar{J}\bar{J}\bar{J}$	12.0	EWD	3	LWD ₁					
2-30	$\bar{U}\bar{J}\bar{J}\bar{J}$	12.0	EWD	3	LWD ₁					
2-31	$\bar{U}\bar{J}\bar{J}\bar{J}$	12.0	EWD	3	LWD ₁					

Table A3. Summary of results for JJJU and JJJŪ. See Sec. 3.1 for a full description of the columns or Table A1 for a summary.

MS = main sequence, GB = giant branch, EWD = white dwarf with 0-100 Myr cooling, LWD = white dwarf beyond 100 Myr cooling.
Notes:

^aSubsequent evolution may have been affected by tides on the GB phase.

^bSubsequent evolution may have been affected by tides on the MS phase.

^cSubsequent evolution may have been affected by tides on the WD phase.

Sim #	Setup	β	Unpack	# Surv	Engulf	Eject	Collision	$< R_{\max}$?	TPs Eng	Notes
3-1	JJJU	6.0	EWD	2		EWD ₃ ,EWD ₄				
3-2	JJJU	6.0	EWD	2		EWD ₁ ,EWD ₄		#3 _{1.543}		
3-3	JJJU	6.0	EWD	2		EWD ₂ ,EWD ₄		#3 _{0.743}		a
3-4	JJJU	6.0	EWD	2		EWD ₁ ,EWD ₄				a
3-5	JJJU	6.5	MS	2	MS ₁	MS ₄				b
3-6	JJJU	6.5	MS	2		MS ₄ ,LWD ₃		#1 _{0.505}		
3-7	JJJU	6.5	MS	2	MS ₂	MS ₄				
3-8	JJJU	6.5	MS	2	MS ₁	MS ₄				
3-9	JJJU	7.0	LWD	3		LWD ₄				
3-10	JJJU	7.0	EWD	3		EWD ₄				
3-11	JJJU	7.0	LWD	3		LWD ₄				
3-12	JJJU	7.0	LWD	3		LWD ₄				
3-13	JJJU	7.5		4						
3-14	JJJU	7.5		4						
3-15	JJJU	7.5		4						
3-16	JJJU	7.5		4						
3-17	JJJU	8.0		4						
3-18	JJJU	8.0		4						
3-19	JJJU	8.0		4						
3-20	JJJU	8.0		4						
3-21	JJJŪ	10.0	EWD	3		LWD ₄				
3-22	JJJŪ	10.0	EWD	3		LWD ₄				
3-23	JJJŪ	10.0	LWD	3		LWD ₄				
3-24	JJJŪ	10.0	EWD	3		LWD ₄				
3-25	JJJŪ	11.0	LWD	4				#2 _{0.515} , #4 _{0.00838}		c
3-26	JJJŪ	11.0	LWD	3			LWD ₁₋₃			
3-27	JJJŪ	11.0	LWD	3		LWD ₄				
3-28	JJJŪ	11.0	LWD	3		LWD ₄				
3-29	JJJŪ	12.0	EWD	3		LWD ₄				
3-30	JJJŪ	12.0	EWD	3		LWD ₄				
3-31	JJJŪ	12.0	MS	2		LWD ₄	MS ₁₋₂			
3-32	JJJŪ	12.0	MS	3		LWD ₄				b

Table A4. Summary of results for $\mathcal{U}\mathcal{U}\mathcal{U}\mathcal{J}$ and $\bar{\mathcal{U}}\bar{\mathcal{U}}\bar{\mathcal{U}}\bar{\mathcal{J}}$. See Sec. 3.1 for a full description of the columns or Table A1 for a summary. MS = main sequence, GB = giant branch, EWD = white dwarf with 0-100 Myr cooling, LWD = white dwarf beyond 100 Myr cooling. Notes:

^dA test particle which survived the entire integration achieved a minimum pericentre of 0.0244 au at a WD cooling age of 1.844 Gyr.

^eA test particle which survived the entire integration achieved a minimum pericentre of 0.5537 au at a WD cooling age of 4.446 Gyr.

^fA test particle which survived the entire integration achieved a minimum pericentre of 0.2312 au at a WD cooling age of 6.671 Gyr.

Sim #	Setup	β	Unpack	# Surv	Engulf	Eject	Collision	$< R_{\max}$?	TPs Eng	Notes
4-1	$\mathcal{U}\mathcal{U}\mathcal{U}\mathcal{J}$	7.0	MS	2		MS ₁ ,MS ₂				
4-2	$\mathcal{U}\mathcal{U}\mathcal{U}\mathcal{J}$	7.0	MS	2		MS ₁ ,MS ₂				
4-3	$\mathcal{U}\mathcal{U}\mathcal{U}\mathcal{J}$	7.0	MS	2		MS ₃	MS ₁₋₂			
4-4	$\mathcal{U}\mathcal{U}\mathcal{U}\mathcal{J}$	7.0	MS	1	GB ₁	MS ₂ ,MS ₃				
4-5	$\mathcal{U}\mathcal{U}\mathcal{U}\mathcal{J}$	7.5	MS	2		MS ₂ ,MS ₃				
4-6	$\mathcal{U}\mathcal{U}\mathcal{U}\mathcal{J}$	7.5	MS	2		MS ₂ ,MS ₃				
4-7	$\mathcal{U}\mathcal{U}\mathcal{U}\mathcal{J}$	7.5	MS	2		MS ₃	MS ₁₋₄			
4-8	$\mathcal{U}\mathcal{U}\mathcal{U}\mathcal{J}$	7.5	MS	2		GB ₃	MS ₁₋₂			
4-9	$\mathcal{U}\mathcal{U}\mathcal{U}\mathcal{J}$	8.0	MS	2		MS ₁ ,WD ₂				
4-10	$\mathcal{U}\mathcal{U}\mathcal{U}\mathcal{J}$	8.0	MS	2		MS ₁ ,MS ₂				
4-11	$\mathcal{U}\mathcal{U}\mathcal{U}\mathcal{J}$	8.0	MS	2		MS ₂ ,MS ₃				
4-12	$\mathcal{U}\mathcal{U}\mathcal{U}\mathcal{J}$	8.0	MS	2		MS ₁ ,MS ₃				
4-13	$\mathcal{U}\mathcal{U}\mathcal{U}\mathcal{J}$	8.5	EWD	2		EWD ₂ ,EWD ₃			(8/0)	
4-14	$\mathcal{U}\mathcal{U}\mathcal{U}\mathcal{J}$	8.5	EWD	2		EWD ₂ ,EWD ₃			(12/0)	
4-15	$\mathcal{U}\mathcal{U}\mathcal{U}\mathcal{J}$	8.5	EWD	2		EWD ₂ ,EWD ₃			(12/0)	
4-16	$\mathcal{U}\mathcal{U}\mathcal{U}\mathcal{J}$	8.5	EWD	2		EWD ₂	EWD ₁₋₃		(3/1)	
4-17	$\mathcal{U}\mathcal{U}\mathcal{U}\mathcal{J}$	9.0	LWD	2		LWD ₂ ,LWD ₃			(0/12)	
4-18	$\mathcal{U}\mathcal{U}\mathcal{U}\mathcal{J}$	9.0	LWD	2		LWD ₂ ,LWD ₃		#1 _{0.464}	(0/12)	
4-19	$\mathcal{U}\mathcal{U}\mathcal{U}\mathcal{J}$	9.0	LWD	2		LWD ₁ ,LWD ₃			(0/10)	
4-20	$\mathcal{U}\mathcal{U}\mathcal{U}\mathcal{J}$	9.0	LWD	2		LWD ₂ ,LWD ₃			(0/7)	
4-21	$\mathcal{U}\mathcal{U}\mathcal{U}\mathcal{J}$	9.5	LWD	2		LWD ₁ ,LWD ₂			(0/11)	
4-22	$\mathcal{U}\mathcal{U}\mathcal{U}\mathcal{J}$	9.5	LWD	2		LWD ₁ ,LWD ₂			(0/11)	d
4-23	$\mathcal{U}\mathcal{U}\mathcal{U}\mathcal{J}$	9.5	LWD	2		LWD ₁ ,LWD ₃			(0/11)	
4-24	$\mathcal{U}\mathcal{U}\mathcal{U}\mathcal{J}$	9.5	LWD	2		LWD ₁ ,LWD ₃			(0/10)	e,f
4-25	$\bar{\mathcal{U}}\bar{\mathcal{U}}\bar{\mathcal{U}}\bar{\mathcal{J}}$	10.0	MS	2			MS ₂₋₄ ,LWD ₃₋₄			
4-26	$\bar{\mathcal{U}}\bar{\mathcal{U}}\bar{\mathcal{U}}\bar{\mathcal{J}}$	10.0	MS	3			MS ₂₋₄ ,			
4-27	$\bar{\mathcal{U}}\bar{\mathcal{U}}\bar{\mathcal{U}}\bar{\mathcal{J}}$	10.0	MS	2			MS ₁₋₄ ,MS ₂₋₃			
4-28	$\bar{\mathcal{U}}\bar{\mathcal{U}}\bar{\mathcal{U}}\bar{\mathcal{J}}$	10.0	MS	2			MS ₁₋₄ ,MS ₂₋₄			
4-29	$\bar{\mathcal{U}}\bar{\mathcal{U}}\bar{\mathcal{U}}\bar{\mathcal{J}}$	12.0	MS	4						
4-30	$\bar{\mathcal{U}}\bar{\mathcal{U}}\bar{\mathcal{U}}\bar{\mathcal{J}}$	12.0	MS	3			MS ₁₋₄			
4-31	$\bar{\mathcal{U}}\bar{\mathcal{U}}\bar{\mathcal{U}}\bar{\mathcal{J}}$	12.0	MS	2			MS ₂₋₄ ,MS ₃₋₄			
4-32	$\bar{\mathcal{U}}\bar{\mathcal{U}}\bar{\mathcal{U}}\bar{\mathcal{J}}$	12.0	MS	3			MS ₂₋₄			
4-33	$\bar{\mathcal{U}}\bar{\mathcal{U}}\bar{\mathcal{U}}\bar{\mathcal{J}}$	14.0	LWD	4						
4-34	$\bar{\mathcal{U}}\bar{\mathcal{U}}\bar{\mathcal{U}}\bar{\mathcal{J}}$	14.0	LWD	4						
4-35	$\bar{\mathcal{U}}\bar{\mathcal{U}}\bar{\mathcal{U}}\bar{\mathcal{J}}$	14.0	LWD	4						
4-36	$\bar{\mathcal{U}}\bar{\mathcal{U}}\bar{\mathcal{U}}\bar{\mathcal{J}}$	14.0	LWD	4						

Table A5. Summary of results for JUUJ and J̄ŪŪJ. See Sec. 3.1 for a full description of the columns or Table A1 for a summary. MS = main sequence, GB = giant branch, EWD = white dwarf with 0-100 Myr cooling, LWD = white dwarf beyond 100 Myr cooling. Notes:

^bSubsequent evolution may have been affected by tides on the MS phase.

^cSubsequent evolution may have been affected by tides on the WD phase.

^zUnpacking, ejections and engulfments all occur for WD cooling ages exceeding 10 Gyr.

Sim #	Setup	β	Unpack	# Surv	Engulf	Eject	Collision	$< R_{\max}$?	TPs Eng	Notes
5-1	JUUJ	6.0	MS	2		MS ₂ ,MS ₃				
5-2	JUUJ	6.0	MS	2		MS ₂ ,MS ₃				
5-3	JUUJ	6.0	MS	2		MS ₂ ,MS ₃				
5-4	JUUJ	6.0	MS	2		MS ₂ ,MS ₃				
5-5	JUUJ	6.5	MS	2		MS ₃ ,EWD ₂				
5-6	JUUJ	6.5	MS	2		MS ₂ ,MS ₃				
5-7	JUUJ	6.5	MS	2		MS ₂ ,MS ₃				
5-8	JUUJ	6.5	MS	2		MS ₂ ,MS ₃				
5-9	JUUJ	7.0	LWD	2		LWD ₂ ,LWD ₃				
5-10	JUUJ	7.0	MS	2		MS ₂ ,MS ₃				
5-11	JUUJ	7.0	EWD	2		EWD ₂ ,EWD ₃				
5-12	JUUJ	7.0	MS	2		MS ₂ ,EWD ₃				
5-13	JUUJ	7.5	MS	2		MS ₂ ,MS ₃				
5-14	JUUJ	7.5	MS	2		MS ₂	MS ₁₋₃			
5-15	JUUJ	7.5	MS	2		MS ₂ ,MS ₃				
5-16	JUUJ	7.5	MS	2		MS ₂ ,MS ₃				
5-17	JUUJ	8.0	MS	2		MS ₂ ,MS ₃				
5-18	JUUJ	8.0	MS	2	MS ₂	MS ₃				
5-19	JUUJ	8.0	MS	2		MS ₂ ,MS ₃				
5-20	JUUJ	8.0	MS	2		MS ₂ ,MS ₃				
5-21	JUUJ	8.5	EWD	2		EWD ₂ ,EWD ₃			(2/0)	
5-22	JUUJ	8.5	MS	2		MS ₂ ,MS ₃			(0/0)	
5-23	JUUJ	8.5	EWD	2		EWD ₂ ,EWD ₃			(0/0)	
5-24	JUUJ	8.5	EWD	2		EWD ₂ ,EWD ₃			(0/0)	
5-25	JUUJ	9.0	EWD	2		EWD ₂ ,EWD ₃			(0/0)	
5-26	JUUJ	9.0	EWD	2		EWD ₂ ,EWD ₃			(0/0)	
5-27	JUUJ	9.0	EWD	2		EWD ₂ ,LWD ₃			(0/2)	
5-28	JUUJ	9.0	EWD	2		EWD ₂ ,EWD ₃			(4/0)	
5-29	JUUJ	9.5	LWD	2		LWD ₂ ,LWD ₃			(0/3)	
5-30	JUUJ	9.5		4					(0/0)	
5-31	JUUJ	9.5	LWD	2		LWD ₂ ,LWD ₃			(0/2)	
5-32	JUUJ	9.5	LWD	2		LWD ₂ ,LWD ₃			(0/3)	z
5-33	J̄ŪŪJ	10.0	MS	3			MS ₁₋₂			
5-34	J̄ŪŪJ	10.0	MS	3			LWD ₁₋₄			
5-35	J̄ŪŪJ	10.0	MS	2		LWD ₂	LWD ₁₋₄			
5-36	J̄ŪŪJ	10.0	MS	4				#31.624		
5-37	J̄ŪŪJ	12.0	LWD	3		LWD ₂				
5-38	J̄ŪŪJ	12.0	MS	3			GB ₂₋₄			
5-39	J̄ŪŪJ	12.0	MS	3			GB ₁₋₂			
5-40	J̄ŪŪJ	12.0	EWD	4						
5-41	J̄ŪŪJ	14.0	LWD	3			LWD ₁₋₂			
5-42	J̄ŪŪJ	14.0	LWD	4						
5-43	J̄ŪŪJ	14.0	LWD	4						
5-44	J̄ŪŪJ	14.0		4						

Table A6. Summary of results for UJJU and $\bar{U}\bar{J}\bar{J}\bar{U}$. See Sec. 3.1 for a full description of the columns or Table A1 for a summary. MS = main sequence, GB = giant branch, EWD = white dwarf with 0-100 Myr cooling, LWD = white dwarf beyond 100 Myr cooling.

Sim #	Setup	β	Unpack	# Surv	Engulf	Eject	Collision	$< R_{\max}$?	TPs Eng	Notes
6-1	UJJU	6.0	EWD	2		EWD ₁ ,EWD ₄				
6-2	UJJU	6.0	EWD	2		EWD ₁ ,EWD ₄				
6-3	UJJU	6.0	EWD	2	EWD ₁	EWD ₄				
6-4	UJJU	6.0	EWD	2		EWD ₁ ,EWD ₄				
6-5	UJJU	6.5	MS	2		MS ₁ ,MS ₄				
6-6	UJJU	6.5	MS	2		MS ₁ ,MS ₄				
6-7	UJJU	6.5	MS	2	MS ₁	MS ₄				
6-8	UJJU	6.5	MS	2		MS ₁ ,MS ₄				
6-9	UJJU	7.0		4						
6-10	UJJU	7.0	LWD	2		LWD ₁ ,LWD ₄				
6-11	UJJU	7.0		4						
6-12	UJJU	7.0		4						
6-13	UJJU	7.5		4						
6-14	UJJU	7.5		4						
6-15	UJJU	7.5		4						
6-16	UJJU	7.5		4						
6-17	UJJU	8.0		4						
6-18	UJJU	8.0		4						
6-19	UJJU	8.0		4						
6-20	UJJU	8.0		4						
6-21	$\bar{U}\bar{J}\bar{J}\bar{U}$	9.0	EWD	3			LWD ₂₋₃			
6-22	$\bar{U}\bar{J}\bar{J}\bar{U}$	9.0	MS	3			MS ₁₋₃			
6-23	$\bar{U}\bar{J}\bar{J}\bar{U}$	9.0	LWD	3			LWD ₂₋₃			
6-24	$\bar{U}\bar{J}\bar{J}\bar{U}$	9.0	MS	2		LWD ₁	MS ₂₋₄			
6-25	$\bar{U}\bar{J}\bar{J}\bar{U}$	10.0	LWD	4						
6-26	$\bar{U}\bar{J}\bar{J}\bar{U}$	10.0	LWD	4						
6-27	$\bar{U}\bar{J}\bar{J}\bar{U}$	10.0	LWD	4						
6-28	$\bar{U}\bar{J}\bar{J}\bar{U}$	10.0		4						
6-29	$\bar{U}\bar{J}\bar{J}\bar{U}$	11.0	LWD	4						
6-30	$\bar{U}\bar{J}\bar{J}\bar{U}$	11.0	LWD	3		LWD ₄				
6-31	$\bar{U}\bar{J}\bar{J}\bar{U}$	11.0	EWD	4						
6-32	$\bar{U}\bar{J}\bar{J}\bar{U}$	11.0	LWD	4						#1 _{1.696}

Table A7. Summary of results for JSUN and $\bar{J}\bar{S}\bar{U}\bar{N}$. See Sec. 3.1 for a full description of the columns or Table A1 for a summary. MS = main sequence, GB = giant branch, EWD = white dwarf with 0-100 Myr cooling, LWD = white dwarf beyond 100 Myr cooling. Notes:
^aSubsequent evolution may have been affected by tides on the GB phase.

Sim #	Setup	β	Unpack	# Surv	Engulf	Eject	Collision	$< R_{\max}$?	TPs Eng	Notes
7-1	JSUN	6.0	MS	2		MS ₃ ,MS ₄				
7-2	JSUN	6.0	MS	2		MS ₃ ,WD ₄				
7-3	JSUN	6.0	MS	2		MS ₃ ,MS ₄				
7-4	JSUN	6.0	EWD	2		EWD ₃ ,EWD ₄				
7-5	JSUN	6.5	MS	2		MS ₃ ,MS ₄				
7-6	JSUN	6.5	EWD	1		EWD ₃ ,EWD ₄ ,LWD ₂				
7-7	JSUN	6.5	MS	2		MS ₃ ,MS ₄				
7-8	JSUN	6.5	MS	2		MS ₃ ,MS ₄				
7-9	JSUN	7.0	MS	2	MS ₄	MS ₃				
7-10	JSUN	7.0	MS	2		EWD ₄	MS ₃₋₄			
7-11	JSUN	7.0	MS	1		MS ₃ ,MS ₄ ,LWD ₂				
7-12	JSUN	7.0	MS	2		MS ₃ ,MS ₄				
7-13	JSUN	7.5	MS	2		MS ₃ ,MS ₄				
7-14	JSUN	7.5	MS	2		MS ₄	MS ₁₋₃			
7-15	JSUN	7.5	MS	2		MS ₃ ,MS ₄				
7-16	JSUN	7.5	MS	2		MS ₃ ,LWD ₄				
7-17	JSUN	8.0	EWD	2		EWD ₃ ,LWD ₄				
7-18	JSUN	8.0	EWD	2		EWD ₃ ,EWD ₄				
7-19	JSUN	8.0	LWD	2		LWD ₃ ,LWD ₄				
7-20	JSUN	8.0	EWD	1		EWD ₃ ,LWD ₂ ,LWD ₄				
7-21	JSUN	8.5		4						(0/0)
7-22	JSUN	8.5	LWD	2		LWD ₃ ,LWD ₄				(0/2)
7-23	JSUN	8.5	LWD	3		LWD ₃				(0/3)
7-24	JSUN	8.5		4						(0/0)
7-25	JSUN	9.0		4						(0/0)
7-26	JSUN	9.0		4						(0/0)
7-27	JSUN	9.0		4						(0/0)
7-28	JSUN	9.0		4						(0/0)
7-29	JSUN	9.5		4						(0/0)
7-30	JSUN	9.5		4						(0/0)
7-31	JSUN	9.5		4						(0/0)
7-32	JSUN	9.5		4						(0/0)
7-33	$\bar{J}\bar{S}\bar{U}\bar{N}$	10.0	MS	2		MS ₃ ,LWD ₂				
7-34	$\bar{J}\bar{S}\bar{U}\bar{N}$	10.0	MS	4						
7-35	$\bar{J}\bar{S}\bar{U}\bar{N}$	10.0	MS	3			MS ₂₋₄			
7-36	$\bar{J}\bar{S}\bar{U}\bar{N}$	10.0	MS	2			MS ₁₋₂ ,LWD ₁₋₄			
7-37	$\bar{J}\bar{S}\bar{U}\bar{N}$	11.0	MS	4						
7-38	$\bar{J}\bar{S}\bar{U}\bar{N}$	11.0	MS	3			MS ₂₋₄			
7-39	$\bar{J}\bar{S}\bar{U}\bar{N}$	11.0	MS	4			MS ₂₋₄			
7-40	$\bar{J}\bar{S}\bar{U}\bar{N}$	11.0	EWD	4						
7-41	$\bar{J}\bar{S}\bar{U}\bar{N}$	12.0	MS	3			LWD ₁₋₄			
7-42	$\bar{J}\bar{S}\bar{U}\bar{N}$	12.0	MS	3			MS ₁₋₃			
7-43	$\bar{J}\bar{S}\bar{U}\bar{N}$	12.0	MS	3			MS ₁₋₄			
7-44	$\bar{J}\bar{S}\bar{U}\bar{N}$	12.0	MS	4				#3 _{0.914} , #4 _{0.455}		a

Table A8. Summary of results for JSNU and $\bar{J}\bar{S}\bar{N}\bar{U}$. See Sec. 3.1 for a full description of the columns or Table A1 for a summary. MS = main sequence, GB = giant branch, EWD = white dwarf with 0-100 Myr cooling, LWD = white dwarf beyond 100 Myr cooling.

Sim #	Setup	β	Unpack	# Surv	Engulf	Eject	Collision	$< R_{\max}$?	TPs Eng	Notes
8-1	JSNU	6.0	MS	2		MS ₃ ,MS ₄				
8-2	JSNU	6.0	MS	2		MS ₃ ,MS ₄				
8-3	JSNU	6.0	MS	2		MS ₃ ,MS ₄				
8-4	JSNU	6.0	MS	2		MS ₃ ,MS ₄				
8-5	JSNU	6.5	MS	2		MS ₂ ,MS ₄				
8-6	JSNU	6.5	MS	2		MS ₃ ,MS ₄				
8-7	JSNU	6.5	EWD	2		EWD ₃ ,EWD ₄				
8-8	JSNU	6.5	EWD	2		EWD ₃ ,EWD ₄				
8-9	JSNU	7.0	MS	2		MS ₃ ,MS ₄				
8-10	JSNU	7.0	MS	2		MS ₃ ,MS ₄				
8-11	JSNU	7.0	MS	2		MS ₃ ,EWD ₄				
8-12	JSNU	7.0	MS	2		MS ₃ ,MS ₄				
8-13	JSNU	7.5	MS	2	MS ₄	MS ₃				
8-14	JSNU	7.5	MS	2		MS ₃ ,MS ₄				
8-15	JSNU	7.5	MS	2		MS ₃	MS ₁₋₄			
8-16	JSNU	7.5	MS	2		MS ₃ ,MS ₄				
8-17	JSNU	8.0	LWD	2		LWD ₂ ,LWD ₄				
8-18	JSNU	8.0	LWD	2		LWD ₃ ,LWD ₄				
8-19	JSNU	8.0	EWD	2		LWD ₃ ,LWD ₄				
8-20	JSNU	8.0	EWD	2		EWD ₄ ,LWD ₃				
8-21	JSNU	8.5	LWD	2		LWD ₃ ,LWD ₄				(0/0)
8-22	JSNU	8.5	LWD	2		LWD ₃ ,LWD ₄				(0/8)
8-23	JSNU	8.5	LWD	2		LWD ₃ ,LWD ₄				(0/1)
8-24	JSNU	8.5	EWD	1		LWD ₂ ,LWD ₃ ,LWD ₄				(4/2)
8-25	JSNU	9.0		4						(0/0)
8-26	JSNU	9.0		4						(0/0)
8-27	JSNU	9.0		4						(0/0)
8-28	JSNU	9.0		4						(0/0)
8-29	JSNU	9.5		4						(0/0)
8-30	JSNU	9.5		4						(0/0)
8-31	JSNU	9.5		4						(0/0)
8-32	JSNU	9.5		4						(0/0)
8-33	$\bar{J}\bar{S}\bar{N}\bar{U}$	10.0	MS	3			LWD ₁₋₂			
8-34	$\bar{J}\bar{S}\bar{N}\bar{U}$	10.0	MS	3			LWD ₁₋₂			
8-35	$\bar{J}\bar{S}\bar{N}\bar{U}$	10.0	MS	2			MS ₁₋₂ ,MS ₁₋₃			
8-36	$\bar{J}\bar{S}\bar{N}\bar{U}$	10.0	MS	3			MS ₂₋₄			
8-37	$\bar{J}\bar{S}\bar{N}\bar{U}$	11.0	MS	2			MS ₁₋₂ ,MS ₁₋₃			
8-38	$\bar{J}\bar{S}\bar{N}\bar{U}$	11.0	MS	3		LWD ₄				
8-39	$\bar{J}\bar{S}\bar{N}\bar{U}$	11.0	MS	3			MS ₁₋₃			
8-40	$\bar{J}\bar{S}\bar{N}\bar{U}$	11.0	MS	3			MS ₁₋₂			
8-41	$\bar{J}\bar{S}\bar{N}\bar{U}$	12.0	MS	4						
8-42	$\bar{J}\bar{S}\bar{N}\bar{U}$	12.0	MS	3			GB ₁₋₂			
8-43	$\bar{J}\bar{S}\bar{N}\bar{U}$	12.0	EWD	4				#30.835		
8-44	$\bar{J}\bar{S}\bar{N}\bar{U}$	12.0	MS	3			MS ₁₋₂			

Table A9. Summary of results for UNJS and $\bar{\text{UNJS}}$. See Sec. 3.1 for a full description of the columns or Table A1 for a summary.

MS = main sequence, GB = giant branch, EWD = white dwarf with 0-100 Myr cooling, LWD = white dwarf beyond 100 Myr cooling.

Notes:

^aSubsequent evolution may have been affected by tides on the GB phase.

Sim #	Setup	β	Unpack	# Surv	Engulf	Eject	Collision	$< R_{\text{max}}?$	TPs Eng	Notes
9-1	UNJS	6.0	MS	2		MS ₁ ,LWD ₂				
9-2	UNJS	6.0	MS	2		MS ₁ ,MS ₂				
9-3	UNJS	6.0	MS	2		MS ₁ ,MS ₂				
9-4	UNJS	6.0	MS	3			MS ₃₋₄			
9-5	UNJS	6.5	EWD	2		EWD ₁ ,EWD ₂				
9-6	UNJS	6.5	MS	2		MS ₁ ,MS ₂				
9-7	UNJS	6.5	MS	2		MS ₁ ,MS ₂				
9-8	UNJS	6.5	EWD	2		EWD ₁ ,LWD ₂				
9-9	UNJS	7.0	EWD	2		EWD ₁ ,EWD ₂				
9-10	UNJS	7.0	EWD	2		EWD ₁ ,EWD ₂				
9-11	UNJS	7.0	EWD	2		EWD ₁ ,EWD ₂				
9-12	UNJS	7.0	EWD	2		EWD ₂ ,LWD ₁				
9-13	UNJS	7.5	MS	2		MS ₂ ,LWD ₄				
9-14	UNJS	7.5	MS	3		MS ₁				
9-15	UNJS	7.5	MS	2		MS ₁ ,LWD ₄				
9-16	UNJS	7.5	MS	1		MS ₁ ,LWD ₂ ,LWD ₄				
9-17	UNJS	8.0	MS	3		MS ₁				
9-18	UNJS	8.0	MS	3			MS ₁₋₂			
9-19	UNJS	8.0	MS	3			MS ₁₋₂			
9-20	UNJS	8.0	MS	1	MS ₂	MS ₁ ,MS ₄				
9-21	UNJS	8.5	EWD	3		EWD ₁			(0/1)	
9-22	UNJS	8.5	EWD	3		EWD ₂			(8/0)	
9-23	UNJS	8.5	EWD	3		EWD ₁			(8/1)	
9-24	UNJS	8.5	EWD	3		EWD ₂			(6/0)	
9-25	UNJS	9.0	EWD	3		EWD ₂			(2/2)	
9-26	UNJS	9.0	EWD	3		EWD ₁			(4/1)	
9-27	UNJS	9.0	EWD	3		EWD ₁			(0/2)	
9-28	UNJS	9.0	EWD	3		EWD ₁			(7/0)	
9-29	UNJS	9.5		4					(0/0)	
9-30	UNJS	9.5		4					(0/0)	
9-31	UNJS	9.5		4					(0/0)	
9-32	UNJS	9.5		4					(0/0)	
9-33	$\bar{\text{UNJS}}$	10.0	MS	2			MS ₂₋₄ ,MS ₃₋₄			
9-34	$\bar{\text{UNJS}}$	10.0	MS	3			GB ₂₋₃			
9-35	$\bar{\text{UNJS}}$	10.0	MS	3			MS ₂₋₃			
9-36	$\bar{\text{UNJS}}$	10.0	MS	4						^a
9-37	$\bar{\text{UNJS}}$	11.0	MS	3			MS ₁₋₃			
9-38	$\bar{\text{UNJS}}$	11.0	MS	4						
9-39	$\bar{\text{UNJS}}$	11.0	MS	4						
9-40	$\bar{\text{UNJS}}$	11.0	MS	4						
9-41	$\bar{\text{UNJS}}$	12.0	MS	3			GB ₁₋₂			
9-42	$\bar{\text{UNJS}}$	12.0	EWD	3			LWD ₃₋₄			
9-43	$\bar{\text{UNJS}}$	12.0	LWD	4						
9-44	$\bar{\text{UNJS}}$	12.0	EWD	4						

Table A10. Summary of results for NUJS and $\bar{N}\bar{U}\bar{J}\bar{S}$. See Sec. 3.1 for a full description of the columns or Table A1 for a summary. MS = main sequence, GB = giant branch, EWD = white dwarf with 0-100 Myr cooling, LWD = white dwarf beyond 100 Myr cooling. Notes:

^aSubsequent evolution may have been affected by tides on the GB phase.

Sim #	Setup	β	Unpack	# Surv	Engulf	Eject	Collision	$< R_{\max}$?	TPs Eng	Notes
10-1	NUJS	7.0	MS	3			MS ₂₋₃			
10-2	NUJS	7.0	MS	2		MS ₁ ,MS ₂				
10-3	NUJS	7.0	MS	3		MS ₂				
10-4	NUJS	7.0	MS	3		MS ₁				
10-5	NUJS	7.5	MS	3		MS ₂				
10-6	NUJS	7.5	MS	2	EWD ₂	MS ₁				
10-7	NUJS	7.5	MS	2	MS ₂	MS ₁				
10-8	NUJS	7.5	MS	2		MS ₂ ,LWD ₁				
10-9	NUJS	8.0	EWD	2		EWD ₁ ,EWD ₂				
10-10	NUJS	8.0	MS	3		MS ₂				
10-11	NUJS	8.0	MS	3		MS ₂				a
10-12	NUJS	8.0	MS	3		MS ₂				
10-13	NUJS	8.5	EWD	3		EWD ₂			(6/0)	
10-14	NUJS	8.5	EWD	3		EWD ₁			(5/0)	
10-15	NUJS	8.5	EWD	3		EWD ₂			(1/3)	
10-16	NUJS	8.5	EWD	3		EWD ₂			(2/1)	
10-17	NUJS	9.0	MS	3		MS ₂			(0/0)	
10-18	NUJS	9.0	EWD	3		EWD ₂			(0/4)	
10-19	NUJS	9.0	EWD	2		EWD ₁ ,EWD ₂			(5/0)	
10-20	NUJS	9.0	EWD	1		EWD ₁ ,EWD ₂ ,LWD ₄			(4/1)	
10-21	NUJS	9.5		4					(0/0)	
10-22	NUJS	9.5		4					(0/0)	
10-23	NUJS	9.5		4					(0/0)	
10-24	NUJS	9.5		4					(0/0)	
10-25	$\bar{N}\bar{U}\bar{J}\bar{S}$	10.0	EWD	3			EWD ₂₋₃			
10-26	$\bar{N}\bar{U}\bar{J}\bar{S}$	10.0	MS	3			MS ₁₋₂			
10-27	$\bar{N}\bar{U}\bar{J}\bar{S}$	10.0	MS	4						
10-28	$\bar{N}\bar{U}\bar{J}\bar{S}$	10.0	MS	3			MS ₃₋₄			
10-29	$\bar{N}\bar{U}\bar{J}\bar{S}$	11.0	MS	3			MS ₁₋₄			
10-30	$\bar{N}\bar{U}\bar{J}\bar{S}$	11.0	MS	3			MS ₃₋₄			
10-31	$\bar{N}\bar{U}\bar{J}\bar{S}$	11.0	MS	3			MS ₁₋₃			a
10-32	$\bar{N}\bar{U}\bar{J}\bar{S}$	11.0	MS	3			MS ₂₋₃			
10-33	$\bar{N}\bar{U}\bar{J}\bar{S}$	12.0	MS	3			LWD ₃₋₄			
10-34	$\bar{N}\bar{U}\bar{J}\bar{S}$	12.0	MS	3			MS ₂₋₃			
10-35	$\bar{N}\bar{U}\bar{J}\bar{S}$	12.0	MS	3			MS ₂₋₄			
10-36	$\bar{N}\bar{U}\bar{J}\bar{S}$	12.0	MS	3			MS ₃₋₄			

Table A11. Summary of results for JUNS and JUNS̄. See Sec. 3.1 for a full description of the columns or Table A1 for a summary. MS = main sequence, GB = giant branch, EWD = white dwarf with 0-100 Myr cooling, LWD = white dwarf beyond 100 Myr cooling. Notes:

^aSubsequent evolution may have been affected by tides on the GB phase.

^dA test particle which survived the entire integration achieved a minimum pericentre of 0.039 au at a WD cooling age of 10.091 Gyr.

^zUnpacking, ejections and engulfments all occur for WD cooling ages exceeding 10 Gyr.

Sim #	Setup	β	Unpack	# Surv	Engulf	Eject	Collision	$< R_{\max}$?	TPs Eng	Notes
11-1	JUNS	7.0	MS	2		MS ₂ ,MS ₃				
11-2	JUNS	7.0	MS	2		MS ₂ ,MS ₃				
11-3	JUNS	7.0	MS	1		MS ₃ ,EWD ₄	MS ₁₋₂			
11-4	JUNS	7.0	MS	2		MS ₂ ,MS ₃				
11-5	JUNS	7.5	MS	2		MS ₂ ,MS ₃				
11-6	JUNS	7.5	MS	2		MS ₂ ,MS ₃				
11-7	JUNS	7.5	MS	2	MS ₃	MS ₂				
11-8	JUNS	7.5	MS	2		MS ₂ ,MS ₃				
11-9	JUNS	8.0	EWD	2		EWD ₃ ,LWD ₂				
11-10	JUNS	8.0	MS	2		MS ₂ ,MS ₃				
11-11	JUNS	8.0	MS	2		MS ₂ ,EWD ₃				
11-12	JUNS	8.0	EWD	2		EWD ₂ ,LWD ₃				
11-13	JUNS	8.5	EWD	2		EWD ₃	EWD ₁₋₂		(0/0)	
11-14	JUNS	8.5	EWD	2		EWD ₂ ,LWD ₃			(4/0)	
11-15	JUNS	8.5	EWD	2		EWD ₂ ,EWD ₃			(2/0)	
11-16	JUNS	8.5	EWD	2		EWD ₂ ,LWD ₃			(1/0)	
11-17	JUNS	9.0	LWD	2		LWD ₂ ,LWD ₃			(0/3)	
11-18	JUNS	9.0	LWD	3		LWD ₂			(0/4)	
11-19	JUNS	9.0		4					(0/1)	
11-20	JUNS	9.0	LWD	2		LWD ₂ ,LWD ₃			(0/1)	
11-21	JUNS	9.5	LWD	3			LWD ₁₋₃		(0/2)	
11-22	JUNS	9.5	LWD	2		LWD ₂ ,LWD ₃			(0/0)	
11-23	JUNS	9.5	LWD	2		LWD ₂ ,LWD ₃			(0/4)	d,z
11-24	JUNS	9.5		4					(0/0)	
11-25	JUNS̄	10.0	MS	4						a
11-26	JUNS̄	10.0	MS	4				#2 _{0.956}		
11-27	JUNS̄	10.0	MS	3			GB ₁₋₂			
11-28	JUNS̄	10.0	MS	4						a
11-29	JUNS̄	11.0	MS	4						
11-30	JUNS̄	11.0	MS	3			MS ₃₋₄			
11-31	JUNS̄	11.0	MS	2			MS ₁₋₃ ,LWD ₁₋₄			
11-32	JUNS̄	11.0	MS	3			GB ₁₋₄			
11-33	JUNS̄	12.0	EWD	4						
11-34	JUNS̄	12.0	MS	2			MS ₁₋₂ ,LWD ₃₋₄			
11-35	JUNS̄	12.0	MS	4				#3 _{1.764}		
11-36	JUNS̄	12.0	EWD	3			LWD ₁₋₄			

Table A12. Summary of results for initially alternating Jupiters and Saturns. See Sec. 3.1 for a full description of the columns or Table A1 for a summary.

MS = main sequence, GB = giant branch, EWD = white dwarf with 0-100 Myr cooling, LWD = white dwarf beyond 100 Myr cooling.

Notes:

^cSubsequent evolution may have been affected by tides on the WD phase.^kThe simulation ran for just 2.534 Gyr due to the tight orbit of the fourth planet along the white dwarf phase.^lThe simulation ran for just 4.644 Gyr due to the tight orbit of the sixth planet along the white dwarf phase.^mThe simulation ran for just 2.994 Gyr due to the tight orbit of the fifth planet along the white dwarf phase.ⁿThe simulation ran for just 3.823 Gyr due to the tight orbit of the fifth planet along the white dwarf phase.^oThe simulation ran for just 8.433 Gyr due to the tight orbit of the third planet along the white dwarf phase.^pThe simulation ran for just 7.105 Gyr due to the tight orbit of the first planet along the white dwarf phase.

Sim #	Setup	β	Unpack	# Surv	Engulf	Eject	Collision	$< R_{\max}$?	Notes
12-1	JSJS	6.0	EWD	2		EWD ₂ ,EWD ₄			
12-2	JSJS	6.0	EWD	2		EWD ₂ ,EWD ₄			
12-3	JSJS	6.0	EWD	2	EWD ₄	EWD ₂			
12-4	JSJS	6.0	EWD	2		EWD ₂ ,EWD ₄			
12-5	JSJS	7.0	EWD	2		EWD ₂ ,EWD ₄			
12-6	JSJS	7.0	EWD	2		EWD ₂ ,EWD ₄ ,LWD ₃		#1 _{0.428}	
12-7	JSJS	7.0	EWD	2		EWD ₂ ,EWD ₄			
12-8	JSJS	7.0	EWD	3		EWD ₂		#4 _{0.218}	k
12-9	JSJSJS	6.0	EWD	3	EWD ₄	EWD ₂ ,EWD ₆			
12-10	JSJSJS	6.0	MS	2	MS ₂ ,GB ₁	MS ₄ ,MS ₆			
12-11	JSJSJS	6.0	EWD	3	EWD ₂	EWD ₃ ,LWD ₄		#6 _{0.917}	l
12-12	JSJSJS	7.0	EWD	2		EWD ₁ ,EWD ₂ ,EWD ₄ ,LWD ₆			
12-13	JSJSJS	7.0	EWD	2	EWD ₃	EWD ₂ ,EWD ₄ ,EWD ₆			
12-14	JSJSJS	7.0	EWD	1	LWD ₃	EWD ₂ ,EWD ₄ ,EWD ₆ ,LWD ₅			
12-15	JSJSJS	7.0	EWD	3	EWD ₆	EWD ₂ ,EWD ₄			
12-16	JSJSJSJS	6.0	EWD	3	EWD ₁	EWD ₄ ,EWD ₆ ,EWD ₈ ,LWD ₃		#5 _{0.669}	m
12-17	JSJSJSJS	6.0	EWD	3	EWD ₇	EWD ₃ ,EWD ₄ ,EWD ₆ ,EWD ₈		#1 _{0.473} , #5 _{0.354}	n
12-18	JSJSJSJS	6.0	EWD	2		EWD ₁ ,EWD ₂ ,EWD ₅ ,EWD ₆ ,LWD ₃ ,LWD ₄		#7 _{0.381}	
12-19	JSJSJSJS	6.0	MS	2	MS ₆ ,GB ₃	MS ₂ ,MS ₄ ,MS ₇ ,MS ₈			
12-20	JSJSJSJS	7.0	EWD	3		EWD ₁ ,EWD ₄ ,EWD ₈ ,LWD ₇	EWD ₁₋₂		
12-21	JSJSJSJS	7.0	EWD	3		EWD ₄ ,EWD ₅ ,EWD ₆ ,EWD ₇ ,EWD ₈		#2 _{1.566} , #3 _{0.034}	c,o
12-22	JSJSJSJS	7.0	EWD	2		EWD ₂ ,EWD ₃ ,EWD ₄ ,EWD ₈ ,LWD ₅ ,LWD ₆		#1 _{0.171}	c
12-23	JSJSJSJS	7.0	EWD	3	EWD ₆	EWD ₂ ,EWD ₄ ,EWD ₅ ,LWD ₈		#1 _{1.586}	p

Table A13. Summary of results for initially alternating Uranuses and Neptunes. See Sec. 3.1 for a full description of the columns or Table A1 for a summary.

MS = main sequence, GB = giant branch, EWD = white dwarf with 0-100 Myr cooling, LWD = white dwarf beyond 100 Myr cooling.
Notes:

^bSubsequent evolution may have been affected by tides on the MS phase.

^cSubsequent evolution may have been affected by tides on the WD phase.

^qThe simulation ran for just 4.831 Gyr due to the tight orbit of the first planet along the white dwarf phase.

^rThe simulation ran for just 2.196 Gyr due to the very tight orbits of the first and sixth planets along the white dwarf phase.

^sThe simulation ran for just 7.368 Gyr due to the tight orbit of the fourth planet along the white dwarf phase.

^tThe simulation ran for just 2.564 Gyr due to the tight orbit of the fourth planet along the white dwarf phase.

^uThe simulation ran for just 2.078 Gyr due to the tight orbit of the first planet along the white dwarf phase.

^vThe simulation ran for just 1.926 Gyr due to the tight orbit of the eighth planet along the white dwarf phase.

Sim #	Setup	β	Unpack	# Surv	Engulf	Eject	Collision	$< R_{\max}$?	Notes
13-1	UNUN	7.0	EWD	3	EWD ₂			#1 _{1.769} , #3 _{0.00731}	c
13-2	UNUN	7.0	EWD	2		EWD ₂	EWD ₁₋₃	#4 _{0.608}	
13-3	UNUN	7.0	EWD	3	EWD ₂			#1 _{0.797}	
13-4	UNUN	7.0	GB	3	GB ₂				
13-5	UNUN	9.0	LWD	2		LWD ₂	LWD ₁₋₃	#1 _{0.891}	
13-6	UNUN	9.0	LWD	2			LWD ₁₋₂ ,LWD ₁₋₃		
13-7	UNUN	9.0	LWD	2	LWD ₁	LWD ₄		#2 _{0.00935}	c
13-8	UNUN	9.0	LWD	3	LWD ₃				
13-9	UNUNUN	7.0	MS	1	MS ₁ ,GB ₆	MS ₄ ,MS ₅	MS ₂₋₃		b
13-10	UNUNUN	7.0	MS	3	MS ₅ ,GB ₆		MS ₂₋₄	#2 _{0.906}	
13-11	UNUNUN	7.0	MS	3	MS ₁		MS ₁₋₃ ,MS ₂₋₄		
13-12	UNUNUN	9.0	EWD	4	LWD ₂	LWD ₆		#1 _{0.784} , #3 _{0.0435}	c,q
13-13	UNUNUN	9.0	EWD	5	LWD ₂			#1 _{0.0424} , #5 _{0.667} , #6 _{0.211}	c,r
13-14	UNUNUN	9.0	EWD	4	LWD ₂	LWD ₁		#3 _{0.238} , #4 _{0.0170} , #5 _{0.0187}	c,s
13-15	UNUNUNUN	9.0	EWD	5	EWD ₃	LWD ₁ ,LWD ₂		#4 _{0.0889} , #8 _{0.153}	c,t
13-16	UNUNUNUN	9.0	EWD	7	LWD ₈			#1 _{0.0121} , #7 _{0.133}	c,u
13-17	UNUNUNUN	9.0	EWD	7	EWD ₁			#3 _{0.213} , #8 _{0.293}	v